MgcRacGAP restricts active RhoA at the cytokinetic furrow and both RhoA and Rac1 at cell–cell junctions in epithelial cells

Elaina B. Breznau[a], Ansley C. Semack[b,*], Tomohito Higashi[b], and Ann L. Miller[a,b]
[a]Program in Cellular and Molecular Biology and [b]Department of Molecular, Cellular, and Developmental Biology, University of Michigan, Ann Arbor, MI 48109

ABSTRACT **Localized activation of Rho GTPases is essential for multiple cellular functions, including cytokinesis and formation and maintenance of cell–cell junctions. Although MgcRacGAP (Mgc) is required for spatially confined RhoA-GTP at the equatorial cortex of dividing cells, both the target specificity of Mgc's GAP activity and the involvement of phosphorylation of Mgc at Ser-386 are controversial. In addition, Mgc's function at cell–cell junctions remains unclear. Here, using gastrula-stage *Xenopus laevis* embryos as a model system, we examine Mgc's role in regulating localized RhoA-GTP and Rac1-GTP in the intact vertebrate epithelium. We show that Mgc's GAP activity spatially restricts accumulation of both RhoA-GTP and Rac1-GTP in epithelial cells—RhoA at the cleavage furrow and RhoA and Rac1 at cell–cell junctions. Phosphorylation at Ser-386 does not switch the specificity of Mgc's GAP activity and is not required for successful cytokinesis. Furthermore, Mgc regulates adherens junction but not tight junction structure, and the ability to regulate adherens junctions is dependent on GAP activity and signaling via the RhoA pathway. Together these results indicate that Mgc's GAP activity down-regulates the active populations of RhoA and Rac1 at localized regions of epithelial cells and is necessary for successful cytokinesis and cell–cell junction structure.**

Monitoring Editor
Jeffrey D. Hardin
University of Wisconsin

Received: Nov 20, 2014
Revised: Apr 14, 2015
Accepted: Apr 30, 2015

INTRODUCTION

The fundamental importance of cytokinesis—the last step of cell division—is evident throughout life. Cytokinesis drives development and helps maintain adult tissues, whereas cytokinesis failure can promote birth defects, tumor formation, and tumor cell invasion (Fujiwara *et al.*, 2005; Lacroix and Maddox, 2012; Godinho *et al.*, 2014). Therefore the mechanisms that regulate cytokinesis must be tightly regulated in space and time to ensure successful cell division (Green *et al.*, 2012). An actomyosin-based contractile ring, which is templated by a microtubule-dependent equatorial zone of active RhoA (RhoA-GTP; Bement *et al.*, 2005), generates the force required to pinch a dividing cell in two. Specific guanine nucleotide exchange factors (GEFs) locally activate Rho GTPases (including RhoA, Rac1, and Cdc42) by driving them into the active, GTP-bound state. GTPase-activating proteins (GAPs) inactivate Rho GTPases by promoting GTP hydrolysis. The balance of local GEFs and GAPs precisely regulates the proper spatial and temporal activation of Rho GTPases. Disruption of this tight regulation leads to severe cellular consequences. For example, misregulation of localized RhoA activity can lead to cytokinesis failure (Miller and Bement, 2009).

Centralspindlin, a complex of the kinesin MKLP1 (also called KIF23 in humans, ZEN-4 in *Caenorhabditis elegans*, and Pavarotti in *Drosophila*) and the GAP MgcRacGAP (Mgc; also called RACGAP1 in humans, CYK-4 in *C. elegans*, and RacGAP50C or tumbleweed in *Drosophila*), is a critical regulator of cytokinesis (Jantsch-Plunger *et al.*, 2000; Mishima *et al.*, 2002). Centralspindlin accumulates on the scaffold of overlapping antiparallel microtubules that is formed at the cell equator and contributes to bundling of the central spindle microtubules (Jantsch-Plunger *et al.*, 2000; Hirose *et al.*, 2001). Centralspindlin recruits and concentrates the GEF Ect2 at the cell

This article was published online ahead of print in MBoC in Press (http://www.molbiolcell.org/cgi/doi/10.1091/mbc.E14-11-1553) on May 6, 2015.
*Present address: Department of Genetics, Cell Biology, and Development, University of Minnesota, Minneapolis, MN 55455.
Address correspondence to: Ann L. Miller (annlm@umich.edu).
Abbreviations used: AJ, adherens junction; DN, dominant negative; GAP, GTPase-activating protein; GBD, GTPase-binding domain; GEF, guanine nucleotide exchange factor; LUT, look-up table; mChe, mCherry; Mgc, MgcRacGAP; MO, morpholino oligonucleotide; Rac1-GTP, active Rac1; RhoA-GTP, active RhoA; ROI, region of interest; TJ, tight junction.

equator, where it locally activates RhoA (Somers and Saint, 2003; Yuce *et al.*, 2005; Nishimura and Yonemura, 2006; Su *et al.*, 2011).

The role of Ect2's GEF activity in activating RhoA at the equatorial cortex is well established; however, the target of Mgc's GAP activity is controversial. For example, in vitro analysis of Mgc from *C. elegans* showed relatively low RhoA GAP activity and high Rac1 and Cdc42 GAP activity; however, based on RNA interference results indicating that Rac1 and Cdc42 were not required for cytokinesis in *C. elegans*, it was proposed that Mgc functions to inactivate RhoA in vivo (Jantsch-Plunger *et al.*, 2000). Consistent with this notion, we previously found that in the large blastomeres of early *Xenopus* embryos (Nieuwkoop and Faber stages 7–8), Mgc's GAP activity is important to mediate "GTPase flux," the rapid cycling of RhoA between the GTP- and GDP-bound forms, in order to maintain a focused RhoA activity zone (Bement *et al.*, 2006; Miller and Bement, 2009). However, others concluded that Mgc's GAP activity is directed toward Rac1 or Cdc42 (Toure *et al.*, 1998; Jantsch-Plunger *et al.*, 2000, Canman *et al.*, 2008; Bastos *et al.*, 2012) or indirectly contributes to activation of RhoA (Loria *et al.*, 2012). In addition, two studies reported that in specific cell types, Mgc's GAP activity is not required at all for cell division (Goldstein *et al.*, 2005; Yamada *et al.*, 2006). Further complicating matters, work in HeLa cells reported that Aurora B phosphorylation of Ser-386 (*Xenopus* numbering is used throughout; this residue is S387 in human) in Mgc's GAP domain could convert the in vitro specificity of Mgc's GAP activity from Rac1/Cdc42 to RhoA (Minoshima *et al.*, 2003). In contrast, recent work found that both recombinant Mgc protein and native Centralspindlin complexes immunoprecipitated from HeLa cells exhibited Rac1/Cdc42 GAP activity rather than RhoA GAP activity and that GAP activity was not modulated by phosphorylation at S386 (Bastos *et al.*, 2012). These researchers also showed that Mgc is important for limiting equatorial Rac1 activity and cell–substrate adhesion at the division site in adherent cultured cells (Bastos *et al.*, 2012). Although there are varying results in the literature regarding MgcRacGAP's GAP specificity, the cellular context that gives rise to these results should be considered and may provide an explanation for the differing conclusions.

Unlike adherent cultured cells, epithelial cells do not make strong cell–substrate adhesions. Instead, they exhibit apicobasal polarity and make adhesive cell–cell junctions, which must be maintained and remodeled during cytokinesis. In this cellular context, precise spatiotemporal regulation of RhoA GTPase activity is required both at the division site and for establishment and maintenance of cell–cell junctions (Braga *et al.*, 1997, 1999; Jou *et al.*, 1998; Yamada and Nelson, 2007; Terry *et al.*, 2010). Of note, the Centralspindlin complex was recently implicated in regulation of cell–cell junctions (Ratheesh *et al.*, 2012; Guillemot *et al.*, 2014). In cultured epithelial cells, Mgc is localized not only at the central spindle but also at cell junctions (Ratheesh *et al.*, 2012; Priya *et al.*, 2013; Guillemot *et al.*, 2014). Furthermore, Mgc appears to play a role in regulating junctional Rho GTPase signaling, as well as the structure and function of cell–cell junctions (Ratheesh *et al.*, 2012; Guillemot *et al.*, 2014). However, it is unclear whether Mgc's GAP activity acts on RhoA and/or Rac1 at junctions or whether Mgc's GAP activity is required for regulating adherens junction (AJ) and/or tight junction (TJ) structure.

Here we investigate the effects of perturbing Mgc's GAP activity during cytokinesis in *Xenopus laevis* embryonic epithelial cells (all experiments were done in gastrula-stage, Nieuwkoop and Faber stages 10–11, embryos unless otherwise stated). This approach allows us to monitor the in vivo dynamics of active populations of RhoA or Rac1 during cytokinesis and at cell–cell junctions by live imaging in a polarized intact epithelium. In experiments in which endogenous Mgc was knocked down and replaced with wild-type (WT) or mutant Mgc expressed at near-endogenous levels, we test whether phosphorylation of Mgc Ser-386 is required for successful cytokinesis. We show that phosphorylation at S386 is not required for cytokinesis in vivo; in fact, a phosphomimetic mutation of this residue phenocopies GAP dead Mgc. Using fluorescent probes for active RhoA and Rac1, we determine how Mgc's GAP activity regulates localized accumulation of RhoA-GTP, active Rac1 (Rac1-GTP), and F-actin at the division site and at cell–cell junctions. We find that Mgc's GAP activity spatially restricts RhoA-GTP at the cleavage furrow and both RhoA-GTP and Rac1-GTP at junctions. Finally, we examine how misregulation of Mgc's GAP activity functionally affects cell–cell junction integrity. We demonstrate that Mgc's GAP activity is required to maintain proper adherens junction structure through the RhoA signaling pathway.

RESULTS

MgcRacGAP's GAP activity is required for cytokinesis in *Xenopus* epithelia but phosphorylation at Ser-386 is not

It was reported that Mgc's GAP specificity is regulated by Aurora B phosphorylation during cytokinesis in HeLa cells (Minoshima *et al.*, 2003). To test whether phosphorylation of Ser-386 is required for cytokinesis in the context of the live, polarized epithelium of *Xenopus* embryos, we generated nonphosphorylatable (MgcS386A) or phosphomimetic (MgcS386E) point mutants of Mgc, as well as a GAP-dead point mutant (MgcR384A; *Xenopus* numbering is used; this residue is R385 in human) in which the catalytic arginine finger was mutated to alanine (Figure 1A and Supplemental Figure S1B). Endogenous Mgc was knocked down with a morpholino oligonucleotide (MO) that targets the 5′ untranslated region (UTR) of Mgc (Miller and Bement, 2009) and replaced with near-endogenous levels of WT or mutant Mgc by microinjecting mRNAs that are MO resistant (Figure 1, A–D, and Supplemental Figure S1, A and C). The level of knockdown in cells that were verified to contain MO based on the presence of an injection marker (farnesylated mCherry [mChe-membrane]) was evaluated by immunofluorescence in fixed embryos. In control embryos, endogenous Mgc was localized at the ingressing cytokinetic furrows and midbodies, as well as at cell–cell junctions (Figure 1B and Supplemental Movie S1). Following MO knockdown, Mgc signal was significantly reduced at both the contractile ring and cell–cell junctions (Figure 1, C and D). Of importance, fluorescently tagged MgcWT and each of the Mgc mutants localized appropriately in live *Xenopus* embryos (Supplemental Figure S1D). Triple green fluorescent protein (3xGFP)–tagged WT or mutant Mgc constructs were expressed in embryos in which endogenous Mgc was knocked down. The 3xGFP-tagged Mgc constructs localized to the equatorial cortex and ingressing furrows during cytokinesis (Supplemental Figure S1D) and to cell–cell junctions when expressed at higher levels (unpublished data). In addition, we and others showed previously that mutations within Mgc's GAP domain do not interfere with its ability to interact with MKLP1 in order to form the Centralspindlin complex (Miller and Bement, 2009; Bastos *et al.*, 2012).

We next used the knockdown and replacement approach to test the effects of the Mgc GAP domain mutants on cytokinesis. Embryos were injected with Mgc MO alone, MO + MgcWT, MO + S386A, MO + S386E, or MO + R384A along with GFP-membrane (farnesylated GFP) as an injection marker and were fixed and stained for nuclei (Figure 1E). Embryos in which Mgc was knocked down exhibited significant cytokinesis defects; 23% of cells were binucleate, and 22% had three or more nuclei (Figure 1, E and F). Cells in Mgc MO-injected embryos were also significantly larger than cells

from control embryos, another indication of cytokinesis failure (Figure 1, E and G). Knockdown and replacement with MgcWT rescued multinucleation and cell width to near-control levels (Figure 1, E–G). If phosphorylation at Ser-386 is required for successful cytokinesis as previously reported (Minoshima *et al.*, 2003), we would expect that mutation of the serine to a nonphosphorylatable alanine would cause cytokinesis failure. However, this was not the case. Instead, replacement with MgcS386A had nearly identical effects to replacement with MgcWT; only a minor fraction of cells were binucleate, and the cell width was similar to cells expressing MgcWT. In contrast, replacement with a phosphomimetic mutant (S386E) led to significantly increased multinucleation and cell size compared with replacement with MgcWT (Figure 1, E–G). In fact, the phenotype from replacement with MgcS386E was very similar to the effect of replacement with the MgcR384A GAP-dead mutant (Figure 1, E–G). Both MO + S386E and MO + R384A rescue the Mgc MO phenotype of three or more nuclei to an intermediate extent. This is likely due to Mgc's GAP-independent functions, including recruiting the GEF Ect2 (Somers and Saint, 2003; Yuce *et al.*, 2005; Nishimura and Yonemura, 2006) and bundling central spindle microtubules (Mishima *et al.*, 2002). However, there is still a significant difference in the number of cells with three or more nuclei in MO + S386E and MO + R384A embryos compared with MO + MgcWT embryos ($p = 0.004$ and 0.0012, respectively; Figure 1F). It was initially surprising that MgcS386E phenocopies MgcR384A. However, consistent with this result, Bastos *et al.* (2012) showed that an MgcS386D mutant exhibited decreased GAP activity in in vitro GTP hydrolysis assays. Furthermore, the crystal structure of the GAP domain of human Mgc demonstrates that the catalytic arginine finger residue, Arg-384, is in close proximity to Ser-386 (Matsuura and Lee, 2013). Therefore the negative charge imposed by the glutamic acid in our S386E mutant may interfere with the catalytic activity of the arginine finger, resulting in a similar GAP-dead phenotype for both R384A and S386E. Taken together, these data support the conclusion that phosphorylation of Ser-386 within Mgc's GAP domain is not required for successful cytokinesis in the *Xenopus* epithelium.

Disruption of MgcRacGAP's GAP activity leads to cytokinesis delay or failure

To investigate the nature of the cytokinesis failure observed in fixed embryos, we carried out live imaging on embryos injected with a probe for F-actin (mChe-UtrCH; Burkel *et al.*, 2007). In control cells, a strong, focused band of F-actin accumulates at the contractile ring (Figure 2A and Supplemental Movie S2). Similar to the immunofluorescence analysis (Figure 1, E–G), live imaging revealed that 55% (16 of 29) of cells in embryos injected with Mgc MO failed cytokinesis (Figure 2B). These cells exhibited weak F-actin accumulation at the contractile ring, consistent with Mgc's essential role in recruiting the GEF Ect2 to activate RhoA and thus actin polymerization (Somers and Saint, 2003; Su *et al.*, 2011). Replacement with MgcWT restored normal furrow formation and F-actin accumulation (Figure 2, A and B, and Supplemental Movie S2). Similarly, replacement with S386A rescued the defect observed in embryos injected with MO alone, and F-actin accumulation appeared normal, further confirming that phosphorylation at Ser-386 is not required for cytokinesis in vivo (Figure 2, A and B, and Supplemental Movie S3). In contrast, replacement with either S386E or R384A resulted in cells with a high percentage of furrow regression (Figure 2, A and B, and Supplemental Movie S3). In some cases, multiple F-actin contractile rings were observed for MO, MO + S386E, and MO + R384A cells, indicating that these cells had failed one or more rounds of cytokinesis, resulting in multipolar spindles (Figure 2B and Supplemental Figure S2A). In cells from MO, MO + S386E, and MO + R384A embryos that did manage to complete cytokinesis successfully, we noted that the cells displayed significant increases in the duration of cytokinesis, from the appearance of the contractile ring to completion of furrow ingression (Figure 2, C and D). For example, in MO + R384A cells, the duration of cytokinesis averaged 792 ± 72 s, compared with 364 ± 40 s for MO + MgcWT. One potential explanation for this result is that the larger cell size of the MO, MO + S386E, and MO + R384A cells leads to longer cytokinesis duration. However, consistent with Carvalho *et al.* (2009), linear regression analysis on cell size and cytokinesis completion time demonstrated that cell size did not correlate with duration of cytokinesis completion ($R^2 = 0.06$–0.24; Supplemental Figure S2B). Taken together, our live-imaging data indicate that Mgc's GAP activity is required for successful cytokinesis, as well as for proper spatiotemporal regulation of F-actin accumulation at the contractile ring.

In epithelial cells, the equatorial RhoA-GTP zone is not focused when MgcRacGAP's GAP activity is disrupted

Disrupting Mgc's GAP activity prevents it from down-regulating active Rho GTPases. The cytokinesis failures and abnormal F-actin accumulation observed in MO, MO + S386E, and MO + R384A cells could be due to aberrantly increased RhoA-GTP, as we observed previously in the large blastomeres of the early *Xenopus* embryo (Miller and Bement, 2009), abnormally increased Rac1-GTP, as observed previously in *C. elegans* embryos and adherent HeLa cells (Bastos *et al.*, 2012; Canman *et al.*, 2008), or a combination of both. To examine these possibilities, we first tested the effects of the Mgc GAP-domain mutants upon dynamic RhoA activity during cytokinesis in *Xenopus* epithelial cells.

To visualize the active, GTP-bound populations of RhoA during cytokinesis, we microinjected a fluorescent probe for RhoA-GTP—the GTPase-binding domain (GBD) of Rhotekin fused to GFP (GFP-rGBD; Benink and Bement, 2005). The effects on RhoA-GTP and F-actin accumulation when Mgc was knocked down and replaced with the MgcWT or the Mgc GAP-domain mutants were monitored in polarized epithelial cells.

In control cells, a focused zone of active RhoA forms at the cell equator after anaphase onset, and RhoA-GTP zones are present at cell–cell boundaries of dividing and nondividing cells, as observed previously (Bement *et al.*, 2005; Miller and Bement, 2009; Ratheesh *et al.*, 2012; Reyes *et al.*, 2014; Figure 3A and Supplemental Movie S4). When Mgc was knocked down or its GAP activity was disrupted, RhoA-GTP localization was perturbed at the cytokinetic furrow (Figure 3A). RhoA-GTP accumulation was also perturbed at cell–cell junctions (Figure 3A; also see later discussion of Figure 5). Mgc MO injection resulted in a significant reduction in the intensity of RhoA-GTP at the cleavage furrow during early ingression (Figure 3, A and B, and Supplemental Movie S4). The width of the RhoA-GTP zone was also significantly reduced in Mgc MO embryos compared with control embryos, although the width of F-actin in the contractile ring was unchanged (Figure 3, C and D). This effect on active RhoA is consistent with other reports showing that depletion of Mgc reduced the amount of active RhoA at the cell equator (Yuce *et al.*, 2005; Miller and Bement, 2009; Wolfe *et al.*, 2009; Loria *et al.*, 2012). Replacement with MgcWT rescued the effects of the Mgc MO, restoring the equatorial RhoA activity zone intensity and the width of RhoA-GTP and F-actin nearly to control levels (Figure 3, A–D, and Supplemental Movie S4). If phosphorylation at Ser-386 were required for Mgc to exhibit GAP activity toward RhoA, we would predict that the nonphosphorylatable (S386A) mutant would cause the RhoA activity zone to increase in intensity and/or breadth.

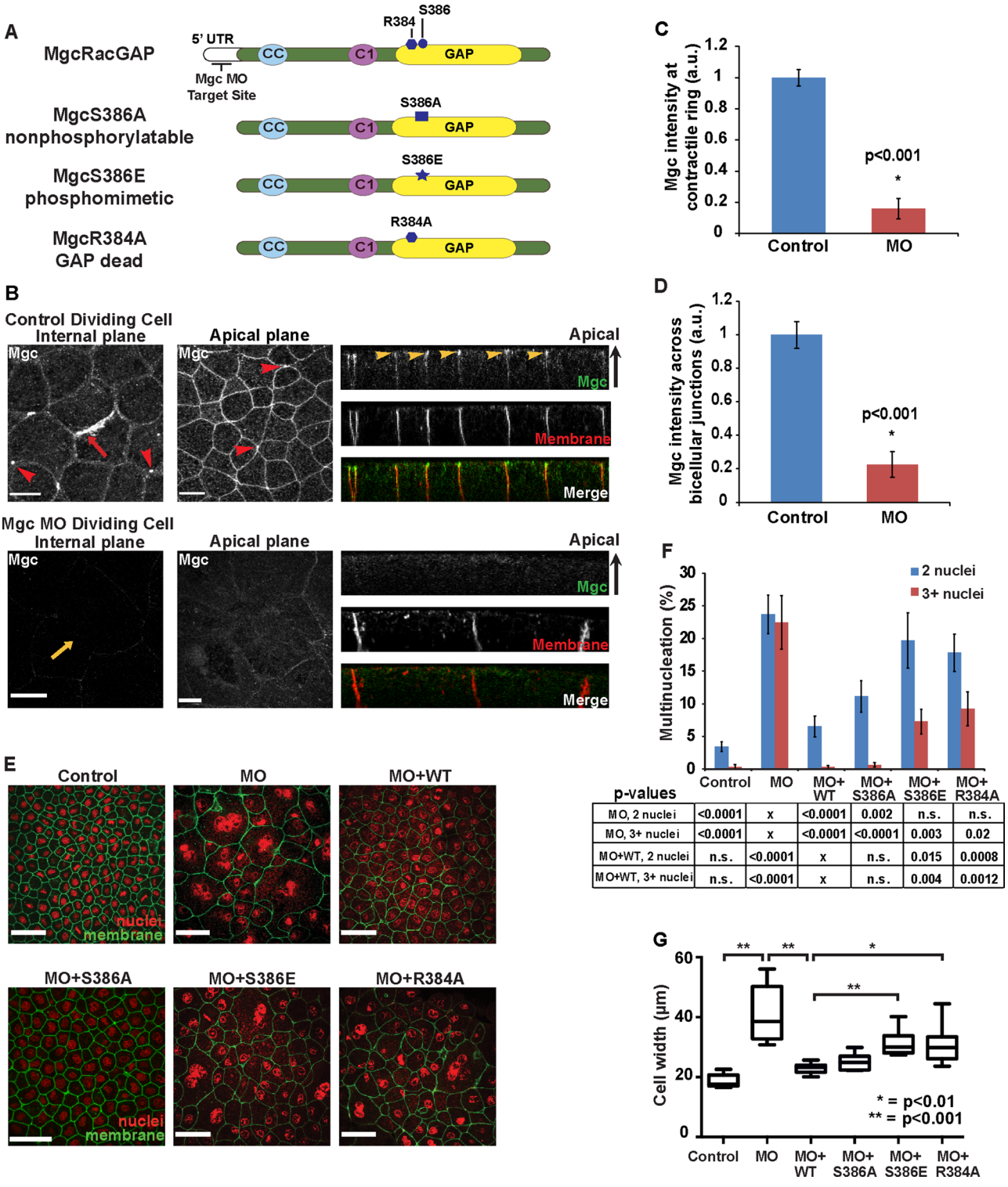

FIGURE 1: MgcRacGAP localizes to cell–cell junctions, and Mgc MO, MO + MgcS386E, and MO + R384A exhibit cytokinesis defects. (A) Protein diagram of Mgc showing location of Arg-384 and Ser-386 within the GAP domain, as well as mutants used in this study. (B) Internal and apical plane en face views and side views of endogenous Mgc localization in fixed embryos injected with either mChe-membrane alone (top) or MO + mChe-membrane (bottom) and then stained with an anti-Mgc antibody. Red arrowheads indicate midbodies; red arrow indicates the contractile ring in control embryo; yellow arrow indicates attempted division site in MO embryo; yellow arrowheads indicate apical localization of endogenous Mgc at cell–cell junctions. Scale bars, 20 µm. (C) Normalized intensity of endogenous Mgc at the contractile ring in control or MO embryos during early ingression measured from embryos that were fixed and stained with an anti-Mgc antibody. Control (number of cells, embryos, and independent experiments, respectively [*n*] = 10, 7, 4), MO (*n* = 11, 7, 4). (D) Peak intensity determined from line scans measuring the normalized Mgc intensity across bicellular junctions. Control (*n* = 20, 5, 4), MO (*n* = 18, 6, 3). (E) Images of fixed embryos injected with

However, no significant differences were observed in RhoA-GTP or F-actin accumulation between MO + MgcWT and MO + S386A cells, providing in vivo evidence that the phosphorylation of Ser-386 is not required for Mgc to act as a RhoA GAP (Figure 3, A–D, and Supplemental Movies S4 and S5). In contrast, in MO + S386E and MO + R384A embryos, we observed significant increases in the intensity of RhoA-GTP at the contractile ring, the width of the RhoA activity zone, and the width of F-actin at the contractile ring (Figure 3, A–D, and Supplemental Movie S5). To confirm that the MgcR384A phenotypes observed in vivo were due to the loss of GAP function and not to an unexpected effect caused by the loss of positive charge from the active site of the GAP domain, we tested an alternate GAP-dead mutant, R384K, which does not alter the charge of the active site (Supplemental Figure S3A; Rittinger *et al.*, 1997a; Miura *et al.*, 2002; Lavelin and Geiger, 2005; Shang *et al.*, 2007). Similar to results with the R384A mutant, cells expressing MO + R384K also fail cytokinesis (Supplemental Figure S3, B and D) and exhibit significantly increased RhoA-GTP intensity at the furrow (Supplemental Figure S3, C and E). Collectively our data provide evidence that despite in vitro data showing that Mgc displays GAP activity primarily toward Rac1 and Cdc42 (Toure *et al.*, 1998; Jantsch-Plunger *et al.*, 2000; Bastos *et al.*, 2012), in an intact epithelial environment, Mgc's GAP activity restricts active RhoA and F-actin accumulation at the division site.

Disruption of MgcRacGAP's GAP activity causes increased accumulation of Rac1-GTP at cell–cell junctions

In adherent cultured cells, Mgc is also important for limiting equatorial Rac1 activity and cell–substrate adhesion in order to achieve successful cytokinesis (Bastos *et al.*, 2012). Genetic data support the idea that Mgc's GAP activity promotes furrow ingression by downregulating Rac1 (D'Avino *et al.*, 2004; Canman *et al.*, 2008). Because the cellular contexts in which these studies were carried out represent different adhesive environments than those experienced by dividing cells in an epithelium in which cell–cell adhesion prevails, we next examined the effects of the Mgc GAP-domain mutants on dynamic Rac1 activity during cytokinesis in the intact epithelium.

To image Rac1-GTP dynamics, we used a fluorescent probe that reports the active, GTP-bound population of Rac1 (GFP-pGBD, the GTPase-binding domain of Pak3 fused to GFP; Miller and Bement, 2009). In vitro binding studies support the use of GFP-pGBD as a reporter for Rac1 activity. First, work identifying effector pathways for RhoA, Rac1, and Cdc42 in HeLa cells showed that Pak1 bound to Rac1 but not Cdc42 in biochemical assays (Bastos *et al.*, 2012). Second, GST-pGBD selectively pulled down Rac1 but not Cdc42 from *Xenopus* tadpole lysates (Li *et al.*, 2002). We monitored the effects on Rac1-GTP and F-actin accumulation when Mgc was knocked down and replaced with the MgcWT or the Mgc GAP-domain mutants in epithelial cells. In control embryos, we did not observe accumulation of Rac1-GTP intensity at the equatorial cortex compared with neighboring cortical regions during early ingression (Figure 4, A and B). However, Rac1-GTP was observed along cell–cell junctions in interphase and dividing cells, and it appeared at the division site during later stages of cytokinesis, where it is likely associated with the formation of nascent cell–cell junctions in the wake of the furrow (Danilchik and Brown, 2008; Herszterg *et al.*, 2013; Figure 4A and Supplemental Movie S6). Injection of Mgc MO alone resulted in no increase in Rac1-GTP at the division site (Figure 4, A and B, and Supplemental Movie S6). Similarly, replacement with MgcWT or the GAP-domain mutants caused no significant changes in the Rac1-GTP intensity at the cleavage furrow (Figure 4, A and B, and Supplemental Movies S6 and S7). Of note, there was no increase in localized Rac1-GTP signal at the cleavage furrow during early ingression when Mgc's GAP activity was disrupted (Figure 4, A and B). This is in contrast to findings in isolated adherent cells, which exhibit increased Rac1 activity at the cleavage furrow in Mgc GAP-dead cells, leading to abnormal cell–substrate adhesion (Bastos *et al.*, 2012), and suggests that in epithelial cells, Mgc's primary target at the division site is not Rac1.

We next analyzed active Rac1 accumulation at cell–cell junctions when Mgc's GAP domain was perturbed. In control embryos, Rac1-GTP localized at cell–cell junctions (Figure 4A and Supplemental Movie S6). Mgc MO embryos exhibited a significant increase in the intensity of active Rac1 at cell–cell junctions, both at bicellular junctions and at vertices where three cells come together, when compared with control embryos (Figure 4, A and C–E, and Supplemental Movie S6). Replacement with MgcWT or MgcS386A rescued the effects of the Mgc MO, restoring the Rac1-GTP activity to control levels at cell–cell junctions (Figure 4, A and C–E, and Supplemental Movies S6 and S7). In contrast, in MO + S386E and MO + R384A embryos, there were significant increases in Rac1-GTP accumulation at cell–cell junctions compared with control or MgcWT embryos (Figure 4, A and C–E, and Supplemental Movie S7). Indeed, quantification demonstrated that the Rac1-GTP signal at junctions in MO, MO + S386E, and MO + R384A embryos was significantly increased in intensity and breadth (measured by full-width at half-maximum) compared with control, MO + MgcWT, or MO + S386A embryos (Figure 4, C–E).

To demonstrate that the signal we observed with the GFP-pGBD probe in live *Xenopus* embryos was specific to Rac1-GTP not Cdc42-GTP, we coinjected the GFP-pGBD probe with a probe for the GTP-bound population of Cdc42 (the GTPase-binding domain of N-WASP [wGBD] fused to monomeric red fluorescent protein [mRFP]; Benink and Bement, 2005; Supplemental Figure S4A). We quantified the accumulation of the probes in control, MO + MgcWT, and MO + R384A embryos and found that GFP-pGBD intensity at cell–cell junctions was increased by nearly twofold in MO + R384A cells compared with control or MO + MgcWT cells (Supplemental Figure S4B). In contrast, there was no increase in mRFP-wGBD intensity in MO + R384A cells (Supplemental Figure S4C). The mRFP-wGBD probe can, however, efficiently detect Cdc42-GTP when Cdc42 is

MO or MO + MgcWT or GAP-domain mutants. mChe-membrane marker (pseudocolored green) was used as an injection marker, and embryos were stained with DAPI (pseudocolored red). Scale bars, 40 μm. (F) Quantification of the percentage of cells that display multinucleation. The *p* values from Student's *t* tests were calculated from comparisons of MO cells with two nuclei or with three or more nuclei pairwise to the respective nuclei group for each indicated construct. The same analysis was conducted for pairwise comparison of MO + WT with two nuclei or with three or more nuclei to each indicated construct. Control ($n = 266, 9, 3$), MO ($n = 184, 9, 6$), MO + WT ($n = 275, 9, 6$), MO + S386A ($n = 247, 8, 5$), MO + S386E ($n = 275, 7, 5$), and MO + R384A ($n = 202, 5, 4$). (G) Quantification of cell width graphed as a box-and-whiskers plot. Control ($n = 333, 6, 3$), MO ($n = 120, 9, 3$), MO + WT ($n = 208, 8, 3$), MO + S386A ($n = 264, 9, 3$), MO+S386E ($n = 207, 7, 3$), and MO+R384A ($n = 219, 10, 3$). All error bars shown represent SEM unless otherwise noted.

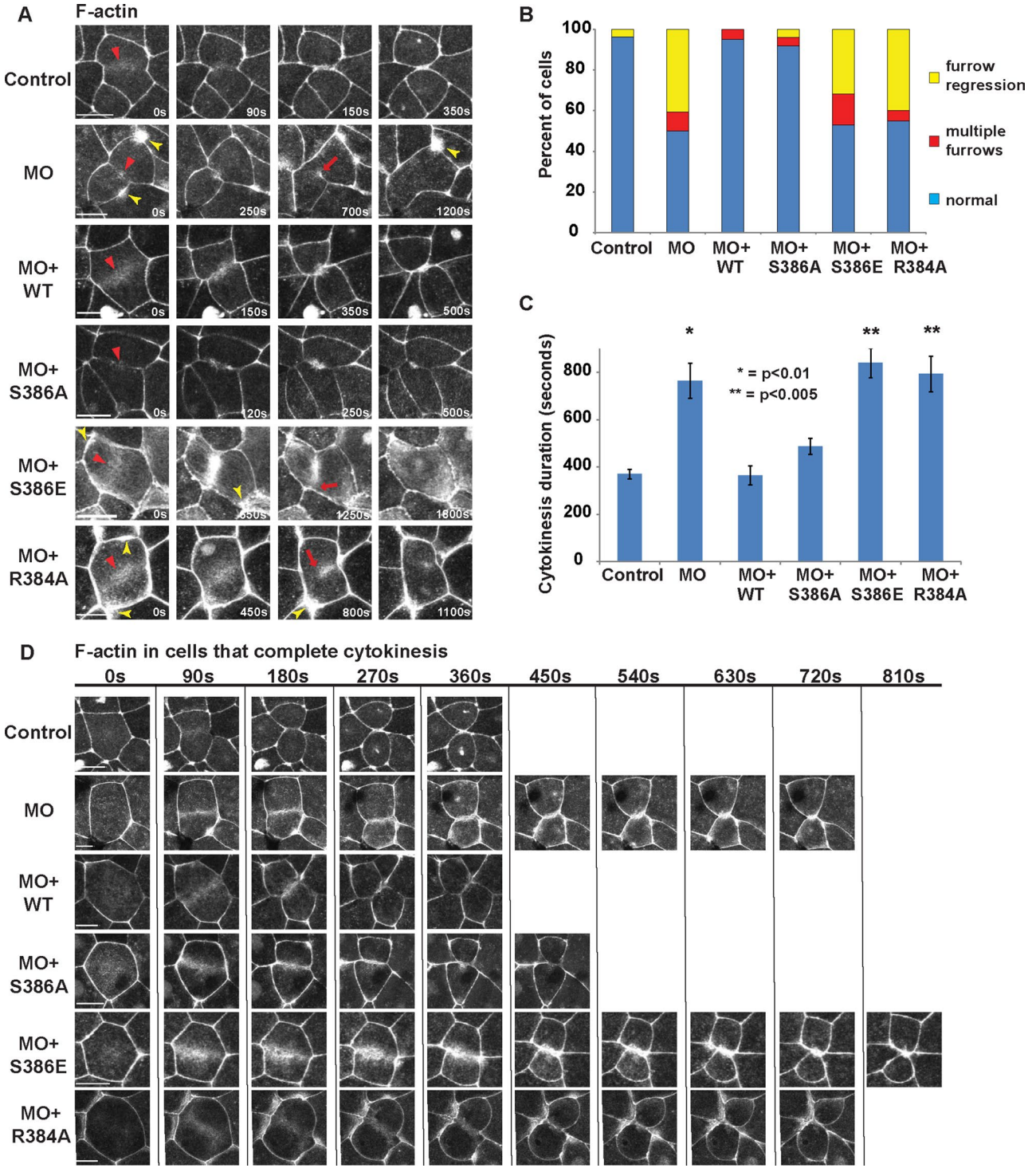

FIGURE 2: Mgc MO, MO + MgcS386E, and MO + MgcR384A exhibit cytokinesis failure and significant delays in cytokinesis completion in vivo. (A) Frames from time-lapse movies during cytokinesis. Embryos were coinjected with the indicated MO and rescue constructs along with mChe-UtrCH (F-actin probe) and mChe-H2B. Red arrowheads point to the contractile ring during early cytokinesis; red arrows indicate cleavage furrow regression; yellow arrowheads point to F-actin–rich junctional accumulations. (B) Quantification of the outcome of cytokinesis showing the percentage of cells that complete cytokinesis normally, fail cytokinesis with cleavage furrow regression, or fail cytokinesis with formation of multiple cleavage furrows. Control (number of cells, embryos, and independent experiments, respectively [*n*] = 26, 9, 4), MO (*n* = 29, 8, 4), MO + WT (*n* = 20, 7, 4), MO + S386A (*n* = 53, 13, 5), MO + S386E (*n* = 48, 12, 5), and MO + R384A (*n* = 19, 3, 3). (C) Quantification of cytokinesis duration. Error bars represent SEM. The *p* values were calculated from pairwise comparison to MO + MgcWT. Control (*n* = 20, 7, 5), MO (*n* = 17, 8, 7), MO + WT (*n* = 17, 11, 7), MO + S386A (*n* = 22, 12, 5), MO+S386E (*n* = 20, 9, 4), and MO + R384A (*n* = 20, 9, 4). (D) Frames from time-lapse movies of cells expressing mChe-UtrCH (F-actin probe) that do manage to complete cytokinesis successfully show that the MO, MO + MgcS386E, and MO + MgcR384A cells display significantly longer cytokinesis duration than control or MO + MgcWT. Scale bars, 20 μm.

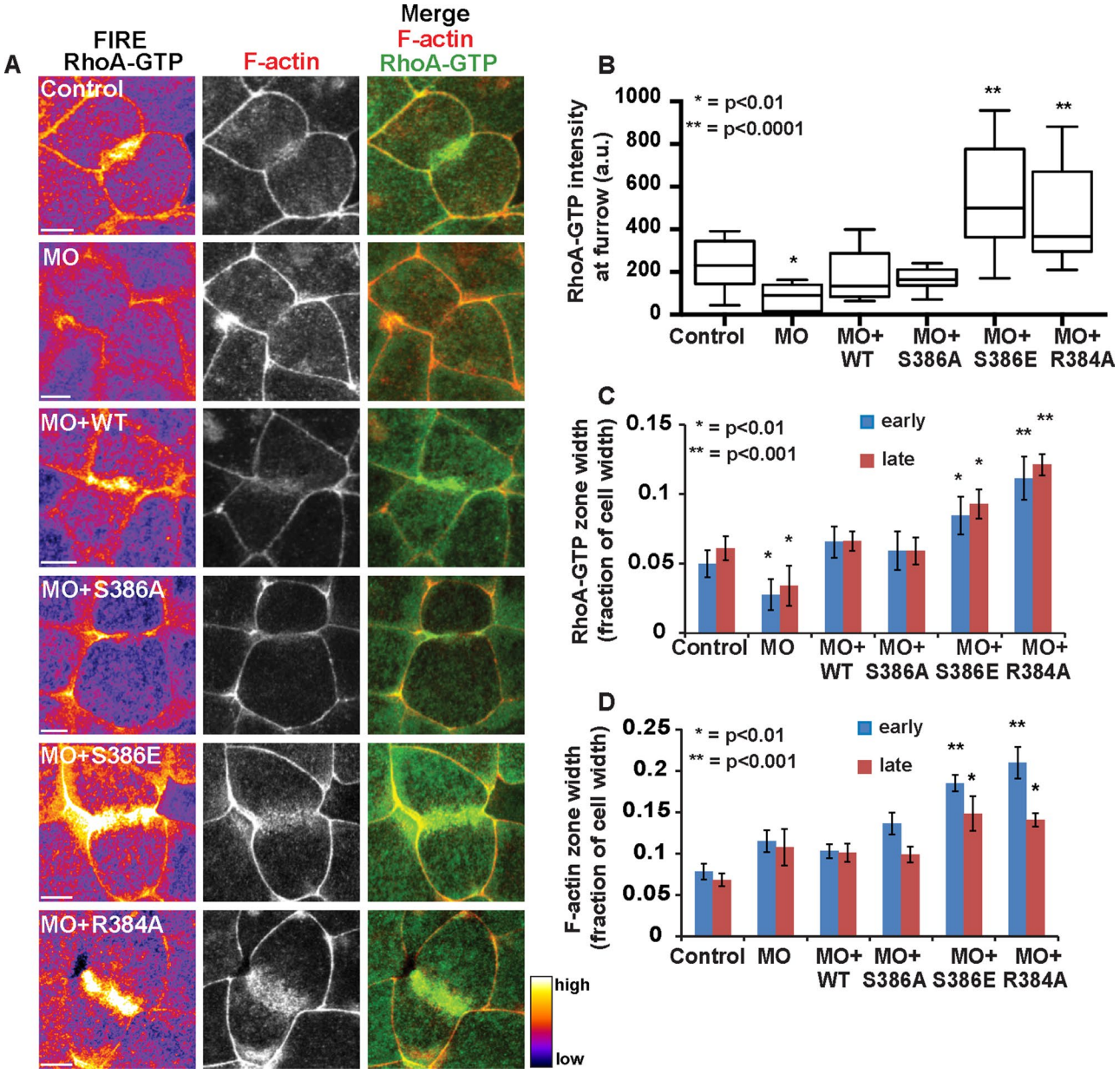

FIGURE 3: MO + MgcS386E and MO + MgcR384A embryos exhibit increased accumulation of RhoA-GTP and F-actin at the contractile ring in epithelial cells. (A) Images of cells during early cytokinesis (~25% ingression) from time-lapse movies, showing the RhoA-GTP zone (GFP-rGBD), with a FIRE look-up table applied to the RhoA-GTP channel, F-actin accumulation (mChe-UtrCH), and merge. Embryos were coinjected with indicated Mgc MO and rescue constructs. Scale bars, 20 µm. (B) Quantification of the normalized RhoA-GTP intensity at the cleavage furrow during early cytokinesis (~25% ingression) graphed as a box-and-whiskers plot. Control (number of cells, embryos, and independent experiments, respectively [*n*] = 14, 3, 2), MO (*n* = 11, 6, 4), MO + WT (*n* = 13, 5, 3), MO + S386A (*n* = 10, 6, 3), MO + S386E (*n* = 17, 6, 2), and MO + R384A (*n* = 18, 5, 3). (C) Quantification of the width of the RhoA-GTP zone as a fraction of overall cell width in both early and late cytokinesis (~25 and 75% ingression, respectively). Control (*n* = 7, 4, 3), MO (*n* = 8, 6, 3), MO + WT (*n* = 8, 6, 5), MO + S386A (*n* = 11, 8, 3), MO + S386E (*n* = 13, 7, 3), and MO + R384A (*n* = 12, 5, 2). (D) Quantification of the width of F-actin accumulation at the contractile ring as a fraction of overall cell width during both early and late cytokinesis (~25 and 75% ingression, respectively). Control (*n* = 7, 4, 3), MO (*n* = 8, 6, 3), MO + WT (*n* = 8, 6, 5), MO + S386A (*n* = 11, 8, 3), MO + S386E (*n* = 13, 7, 3), and MO + R384A (*n* = 12, 5, 2). Error bars represent SEM unless otherwise noted. The *p* values were calculated from pairwise comparison to MO + MgcWT.

activated around plasma membrane wounds generated by laser irradiation in gastrula-stage embryos (Supplemental Figure S4, D–F). Therefore, the negligible mRFP-wGBD signal increase at cell–cell junctions when MgcRacGAP's GAP activity is disrupted allows us to conclude that the signal detected by the GFP-pGBD probe reflects primarily Rac1-GTP. However, we cannot rule out the possibility that the GFP-pGBD probe may detect Cdc42-GTP in some cellular contexts.

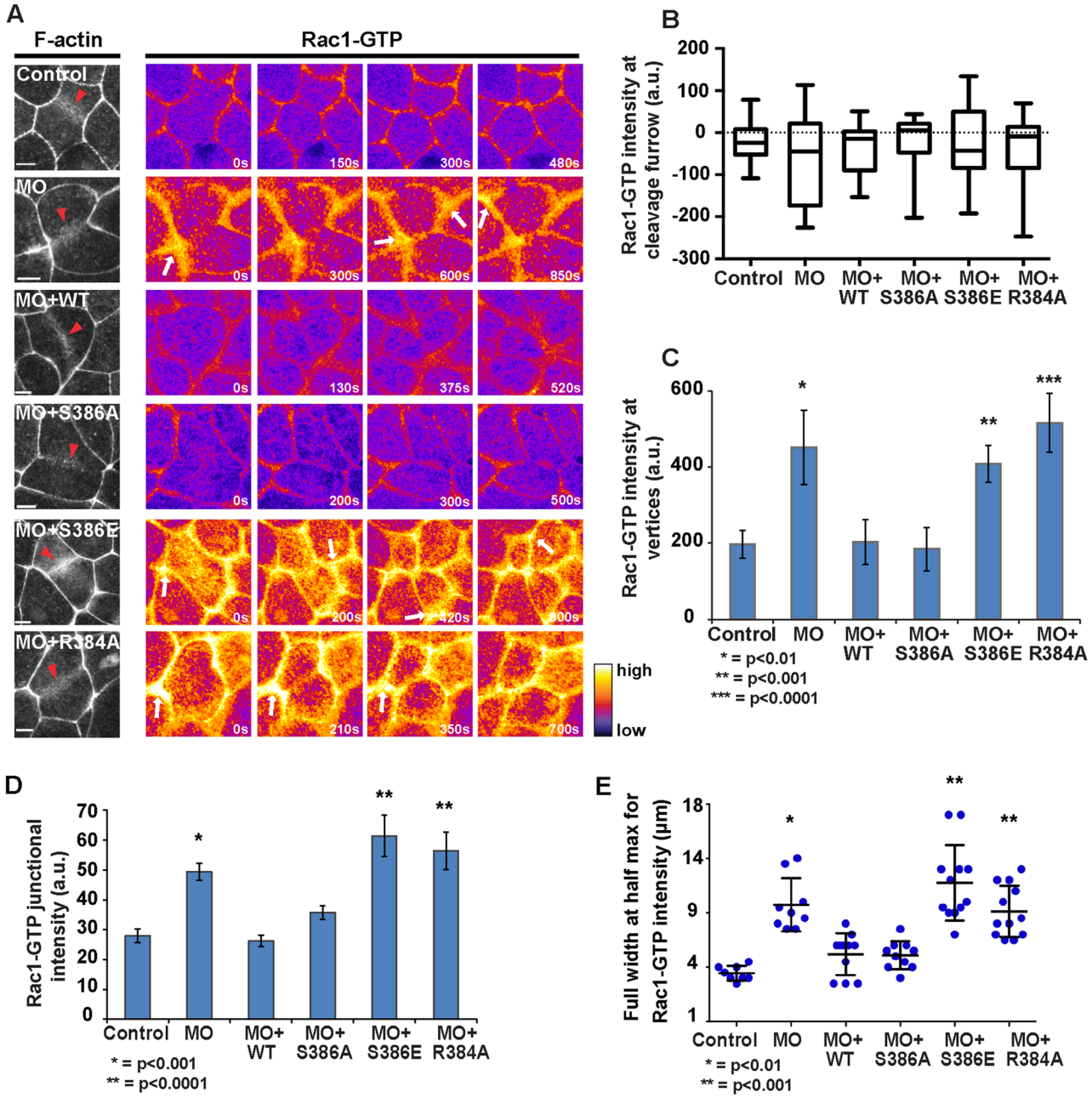

FIGURE 4: Mgc MO, MO + MgcS386E, and MO + MgcR384A embryos exhibit increased accumulation of Rac1-GTP at cell junctions. (A) Frames from time-lapse movies showing F-actin (mChe-UtrCH) at time 0 s (presence of contractile ring indicates dividing cells) and Rac1-GTP in the same cells starting at time 0 s and following cytokinesis over time. Red arrowheads indicate the contractile ring, and white arrows point to regions of Rac1-GTP accumulation. Scale bars, 20 µm. (B) Quantification of the normalized Rac1-GTP intensity at the cleavage furrow during early cytokinesis (~25% cleavage furrow ingression) graphed as a box-and-whiskers plot. A negative value indicates that the Rac1-GTP intensity outside of the cleavage furrow is higher than at the furrow. Control (number of cells, embryos, and independent experiments, respectively [*n*] =18, 4, 4), MO (*n* = 10, 4, 4), MO + WT (*n* = 12, 3, 3), MO + S386A (*n* = 11, 5, 2), MO + S386E (*n* = 14, 5, 4), and MO + R384A (*n* = 15, 5, 4). (C) Quantification of normalized Rac1-GTP intensity measured from an ROI positioned at cell vertices (tricellular junctions). Control (*n* = 12, 3, 3), MO (*n* = 10, 4, 4), MO + WT (*n* = 12, 4, 4), MO + S386A (*n* = 10, 4, 2), MO + S386E (*n* = 22, 5, 3), and MO + R384A (*n* = 16, 7, 4). (D) Quantification of the peak intensity of normalized Rac1-GTP line scans across bicellular junctions of dividing cells during early cleavage furrow ingression. Error bars represent SEM. Control (*n* = 9, 5, 5), MO (*n* = 10, 3, 3), MO + WT (*n* = 11, 6, 5), MO + S386A (*n* = 10, 4, 2), MO + S386E (*n* = 12, 5, 3), and MO + R384A (*n* = 12, 6, 4). (E) Full-width at half-maximum quantification of normalized Rac1-GTP intensity line scans to highlight the difference in breadth of the Rac1-GTP signal across bicellular junctions (see *Materials and Methods*). Error bars represent SEM unless otherwise noted. The *p* values were calculated from pairwise comparisons to MO + MgcWT.

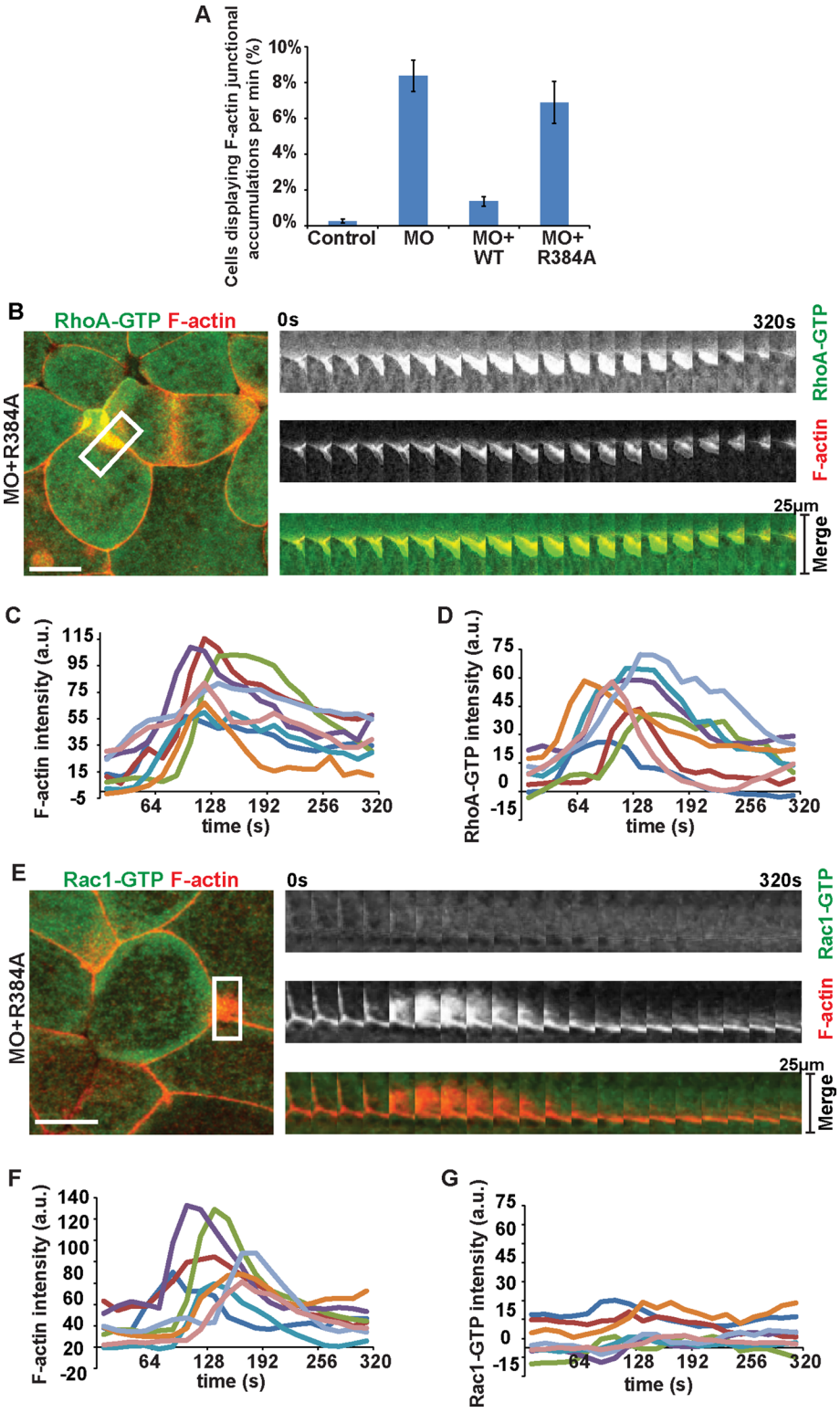

FIGURE 5: Disrupting MgcRacGAP's GAP activity results in dynamic junctional accumulations of F-actin and RhoA-GTP. (A) Quantification of the average percentage of cells with F-actin junctional accumulations per minute. Error bars represent SEM. Control (number of cells, embryos, and independent experiments, respectively [*n*] =335, 10, 8), MO (*n* = 128, 10, 6), MO + WT (*n* = 202, 10, 8), and MO + R384A (*n* = 163, 10, 4). (B) Brightest point projection images were used to generate kymographs across a junction where an F-actin accumulation occurs in MO + R384A embryos. Kymographs of RhoA-GTP (green) and F-actin (red). The white rectangle indicates the region of the kymograph. Scale bar in en face view, 10 μm. (C) Quantification of the normalized F-actin junctional accumulation intensity over time (*n* = 8, 4, 4). (D) Quantification of the normalized RhoA-GTP junctional accumulation intensity over time for the same regions quantified in C. (E) Brightest point projection images were used to generate kymographs across a junction where an F-actin accumulation occurs in MO + R384A embryos. Kymographs of Rac1-GTP (green) and F-actin (red). The white rectangle indicates the region of the kymograph. Scale bar in en face view, 10 μm. (F) Quantification of the normalized F-actin junctional accumulation intensity over time (*n* = 8, 5, 3). (G) Quantification of the normalized Rac1-GTP junctional accumulation intensity over time for the same regions quantified in F. Notice that there is not an increase in local Rac1-GTP intensity at the site of F-actin junctional accumulations.

To complement the knockdown and replacement findings described so far, we overexpressed MgcWT or the Mgc GAP-domain mutants and imaged the accumulation of Rac1-GTP and F-actin at an earlier point in development (Nieuwkoop and Faber stages 6–8; Supplemental Figure S5, A–C). We observed no difference in Rac1-GTP accumulation at junctions in MgcWT or MgcS386A overexpression cells compared with control cells (Supplemental Figure S5, A and B). However, we observed a significant increase in Rac1-GTP at bicellular junctions and cell vertices in embryos in which MgcS386E or MgcR384A were overexpressed compared with control or MgcWT embryos (Supplemental Figure S5, A–C). Taken together, the knockdown and replacement and overexpression studies indicate that Mgc's GAP activity is required to restrict active Rac1 accumulation at cell–cell junctions in epithelial cells.

RhoA-GTP but not Rac1-GTP coaccumulates with dynamic F-actin at cell–cell junctions when MgcRacGAP's GAP activity is disrupted

We observed ectopic F-actin accumulations at cell–cell junctions when Mgc's GAP activity was disrupted (Figure 2A and Supplemental Movies S2, S3, and S8). These F-actin–rich accumulations are significantly increased in frequency in MO + R384A embryos compared with MO + MgcWT embryos (7 ± 1.1% MO + R384A vs. 1 ± 0.2% MO + MgcWT cells/min displayed F-actin–rich accumulations; Figure 5A). We sought to identify the upstream signal promoting these ectopic F-actin accumulations. Two possible explanations are that they could be due to aberrantly increased RhoA-GTP promoting actin polymerization through formins or that they could be due to abnormally increased Rac1-GTP promoting actin polymerization through Arp2/3. Coimaging

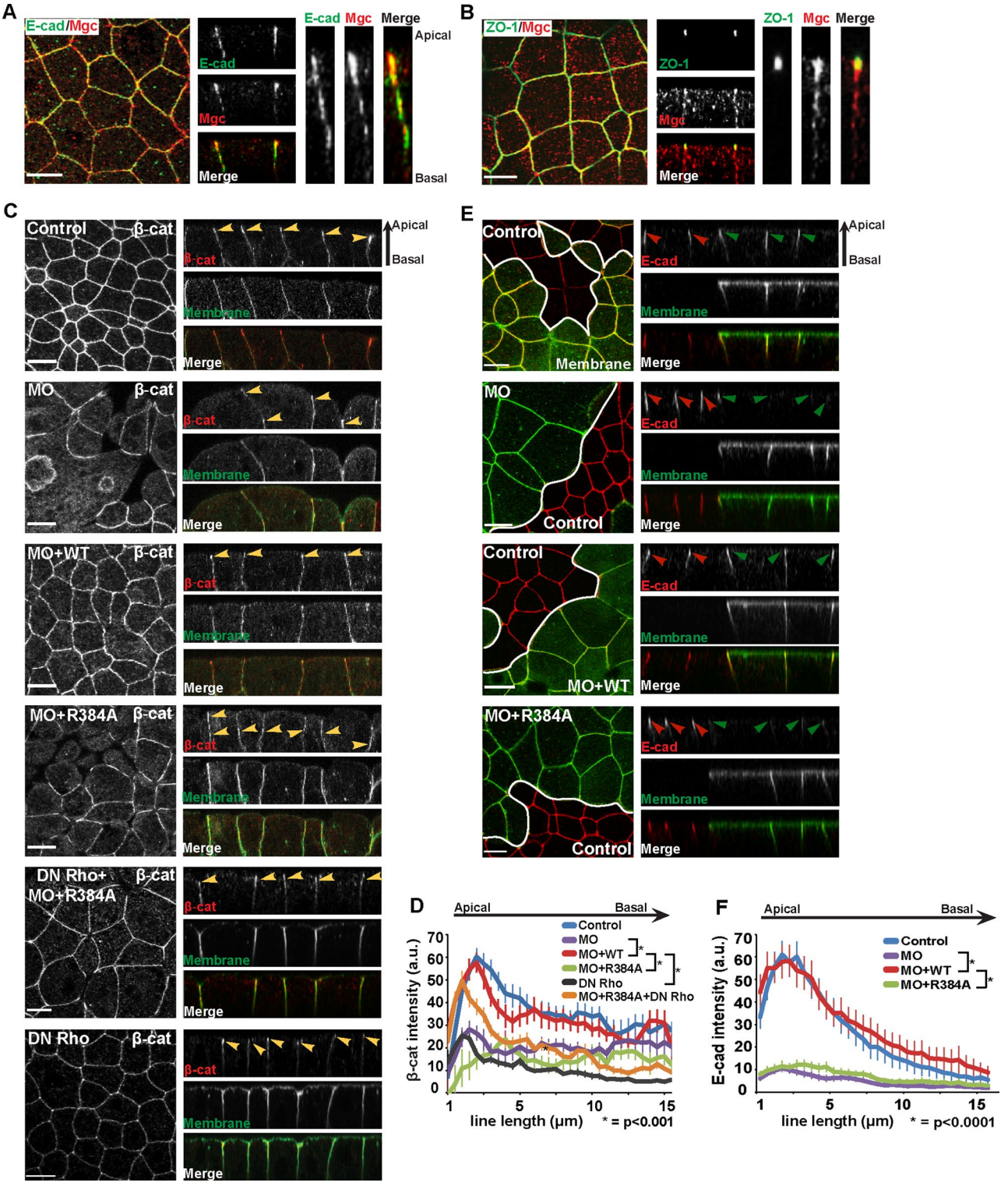

FIGURE 6: MgcRacGAP's GAP activity is required for proper AJ structure. (A, B) Fixed en face and side view images of embryos costained for endogenous Mgc and E-cadherin (A) or Mgc and ZO-1 (B). Side views highlight the overlapping localization (yellow) of Mgc with E-cadherin or Mgc with ZO-1. Scale bars, 20 μm. (C) Fixed en face and side view images of embryos injected with the indicated constructs (MO, MO + MgcWT, MO + R384A, or DN Rho + MO + R384A), as well as GFP-membrane as an injection marker. Embryos were fixed and costained for β-catenin and GFP. Yellow arrowheads indicate concentrated β-catenin localization. Scale bars, 20 μm. (D) Quantification of the normalized β-catenin intensity along the apical-to-basal axis of bicellular junctions. Error bars represent SEM. Control (number of cells, embryos, and independent experiments, respectively [*n*] = 20, 5, 3), MO (*n* = 10, 4, 3), MO + WT (*n* = 18, 4, 3), MO + R384A (*n* = 21, 5, 3), DN Rho + MO + R384A (*n* = 26, 8, 3), and DN Rho (*n* = 28, 10, 3). (E) Still images from live movies showing en face and side view images of mosaic embryos, where all cells in the field of view express E-cadherin–3xmChe, and only the cells expressing GFP-membrane contain marker alone or with MO, MO + MgcWT, or

of F-actin and probes for active RhoA or active Rac1 revealed that RhoA-GTP coaccumulated with the dynamic F-actin–rich structures (Figure 5, B–D, Supplemental Figure S6A, and Supplemental Movie S8). In contrast, Rac1-GTP does not significantly coaccumulate with F-actin–rich junctional accumulations (Figure 5, E–G, Supplemental Figure S6B, and Supplemental Movie S9). These results suggest that the ectopic F-actin–rich junctional accumulations in cells expressing GAP-dead Mgc may be RhoA dependent.

MgcRacGAP's GAP activity is required for proper adherens junction structure in the intact epithelium

Because disrupting Mgc's GAP activity led to misregulation of RhoA-GTP, Rac1-GTP, and F-actin at cell–cell junctions, we next sought to investigate whether Mgc's GAP activity is required for proper junctional structure. It was recently shown that Mgc localizes to cell–cell junctions in cultured epithelial cells, where it appears to play a role in regulating both TJs and AJs (Ratheesh *et al.*, 2012; Guillemot *et al.*, 2014). One study found that Mgc was recruited to AJs by interacting with α-catenin (Ratheesh *et al.*, 2012). In contrast, another study showed that Mgc was localized to TJs via binding to cingulin, a component of TJs, and paracingulin, a component of both TJs and AJs (Guillemot *et al.*, 2014). We examined Mgc's localization at cell–cell junctions in the intact *Xenopus* epithelium. Mgc is enriched at the apical cell–cell junctions (Figure 1 and Supplemental Movie S1) and overlaps significantly with E-cadherin (an AJ transmembrane protein; Figure 6A) and partially with the basal portion of zona occludens 1 (ZO-1; a TJ plaque protein; Figure 6B), indicating that Mgc may localize at the interface between the TJ and the AJ. Mgc is also more weakly localized along the basolateral surface, partially overlapping with lateral E-cadherin signal (Figure 6A).

It is uncertain whether Mgc is required for regulating TJ and/or AJ structure. RhoA and Rac1 play important roles in regulating cell–cell junction formation, maintenance, structure, and function (Braga *et al.*, 1997, 1999; Jou *et al.*, 1998; Machacek *et al.*, 2009; Terry *et al.*, 2010). Because we showed that disrupting Mgc's GAP activity leads to misregulation of both Rac1 (Figure 4) and RhoA (Figure 5) activity at cell–cell junctions, we next tested whether disrupting Mgc's GAP activity affects junction structure. First we examined AJs in fixed *Xenopus* epithelial cells. β-Catenin was apically enriched at AJs in controls (Figure 6, C and D, and Supplemental Figure S8A). However, in Mgc MO embryos, β-catenin was randomly localized along the basolateral surface, and cells were often apically domed (Figure 6, C and D). Reexpression of MgcWT efficiently rescued the β-catenin defect (Figure 6, C and D). Of importance, reexpression of MgcR384A did not rescue, and β-catenin was concentrated at ectopic positions along the basolateral surface rather than polarized at the AJ (Figure 6, C and D, and Supplemental Figure S8B). These data indicate that Mgc's GAP activity is required for proper AJ structure.

We demonstrated that RhoA-GTP coaccumulates with ectopic F-actin–rich structures at cell–cell junctions when Mgc's GAP activity is disrupted (Figure 5), suggesting that these structures might be RhoA dependent. If the effects of Mgc on AJs were mediated through RhoA, we would predict that coexpression of dominant-negative (DN) RhoA in MO + R384A embryos would rescue the AJ defects observed when Mgc's GAP activity is disrupted. Indeed, we observed that coexpression of DN RhoA with MO + R384A partially rescued the AJ defect (Figure 6, C and D), whereas expression of DN Rho alone led to AJ defects similar to MO or MO + R384A treatment (Figure 6, C and D). In contrast, expression of DN Rac did not suppress the junctional defects observed when Mgc's GAP activity was disrupted in MO + R384A embryos (Supplemental Figure S7, A and B). These results support a model in which Mgc's GAP activity regulates the structure of AJs by modulating RhoA-GTP signaling.

To further confirm the effects of Mgc's GAP activity on maintaining the structure of AJs, we tested the effects of Mgc perturbations on E-cadherin, an AJ transmembrane protein. We used live imaging and a mosaic injection strategy in which all cells expressed E-cadherin-3xmChe, and mosaic clones of cells expressed a lineage tracer (GFP-membrane) with or without the MO or MO + Mgc replacement constructs. In control embryos and control regions of mosaic embryos (red arrowheads), E-cadherin was enriched at the AJs, with some localization extending along the lateral membrane (Figure 6, E and F, and Supplemental Figure S8E). Mgc MO embryos exhibited a significant reduction in the intensity of E-cadherin, and this defect was rescued by expression of MgcWT (Figure 6, E and F; green arrowheads). Of importance, MO + R384A embryos showed defects in E-cadherin signal intensity similar to the MO embryos (Figure 6, E and F; green arrowheads). These data, together with the β-catenin studies, indicate that Mgc's GAP activity is important for regulating AJ structure. Our study extends previous work, which identified Mgc as a regulator of AJs (Ratheesh *et al.*, 2012; Priya *et al.*, 2013), by revealing the novel function of Mgc's GAP activity in regulating AJ structure.

MgcRacGAP does not regulate tight junction structure in the intact epithelium

RhoA and Rac1 also play important roles in regulating TJ structure and function (Jou *et al.*, 1998; Terry *et al.*, 2010). Mgc was reported to be recruited to TJs by cingulin and paracingulin and to be involved in regulating TJ barrier formation during junction assembly in Madin–Darby canine kidney cells during calcium-switch experiments (Guillemot *et al.*, 2014). Therefore we next examined whether disrupting Mgc affects TJ structure, by analyzing effects on the TJ proteins claudin (a TJ transmembrane protein) and ZO-1 (a TJ plaque protein). Embryos were injected to generate mosaic regions where internal control cells (red arrowheads) are located next to cells expressing a lineage tracer (GFP-membrane) alone or with Mgc MO (green arrowheads). In control cells, claudin was concentrated at the TJ (Figure 7, A and B, and Supplemental Figure S8C). In mosaic regions where Mgc was knocked down with the MO, claudin signal appeared nearly identical in intensity and apicobasal polarity to controls, even in large cells that had failed multiple rounds of cytokinesis (Figure 7, A and B, and Supplemental Figure S8D). We also stained mosaic embryos for ZO-1. Again, we observed no defect in

MO + R384A. Red arrowheads indicate E-cadherin localization in control regions, and green arrowheads indicate E-cadherin localization in regions expressing the GFP-membrane injection marker and replacement construct as indicated. White lines represent separation between control region and perturbed region. Scale bars, 20 μm.
(F) Quantification of the normalized E-cadherin–3XmChe intensity along the apical-to-basal axis of bicellular junctions. Error bars represent SEM. Control ($n = 21, 8, 2$), MO ($n = 25, 10, 3$), MO + WT ($n = 20, 6, 3$), and MO + R384A ($n = 27, 9, 3$). Significance values were determined using a Student's *t* test comparing the peak intensity value of each indicated construct to the peak value of MO + WT.

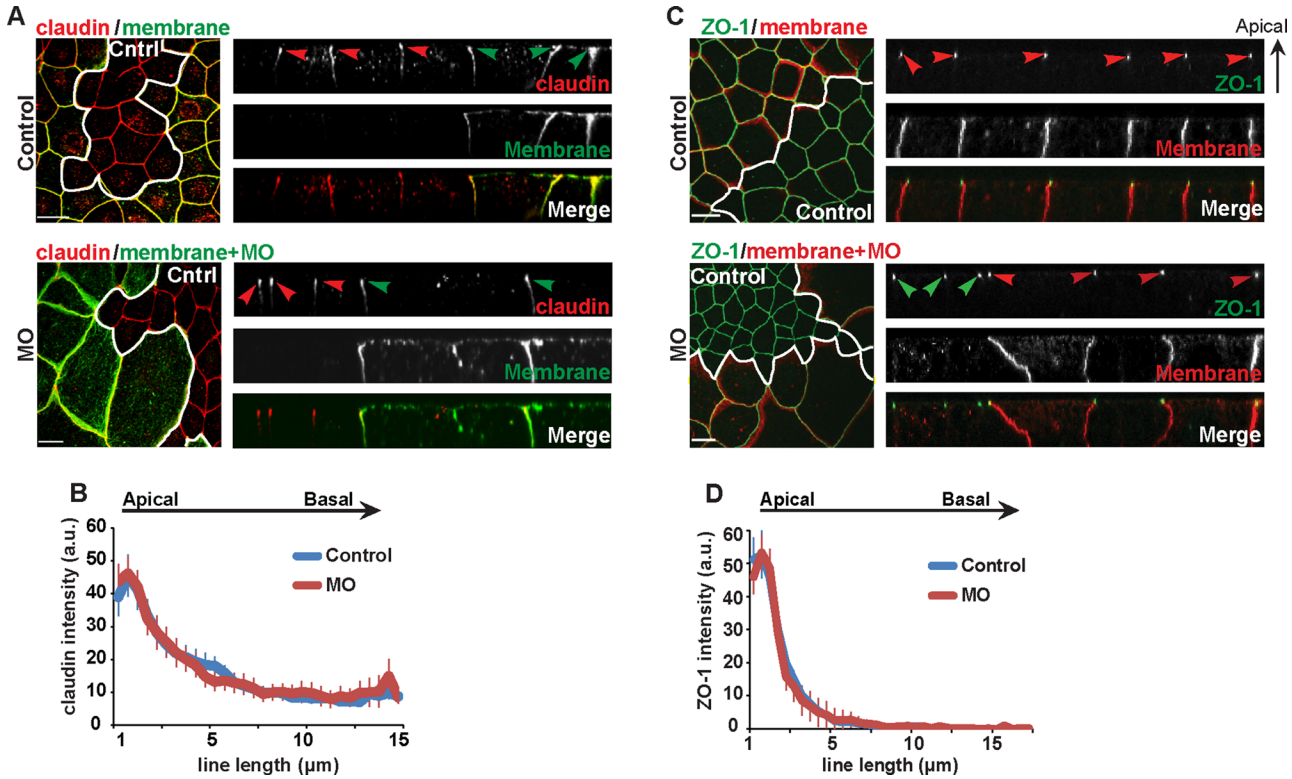

FIGURE 7: MgcRacGAP is not required for proper TJ structure. (A) Fixed en face or side view images of mosaic embryos, where all cells in the field of view are stained for endogenous claudin (red), and the cells expressing GFP-membrane marker (green) contain marker alone (control) or marker + MO (MO). White lines represent separation between mosaic regions. Red arrowheads indicate claudin localization in control regions of the embryo, and green arrowheads indicate claudin localization in regions expressing the injection marker. Scale bars, 20 μm. (B) Quantification of normalized claudin intensity along the apical-to-basal axis of bicellular junctions. Error bars represent SEM. Control (number of cells, embryos, and independent experiments, respectively [*n*] =16, 5, 3), MO (*n* = 14, 5, 3). (C) Fixed en face or side view images of mosaic embryos, where all cells in the field of view are stained for endogenous ZO-1 (green), and the cells expressing mChe-membrane marker (red) contain marker alone (control) or marker + MO (MO). White lines represent separation between mosaic regions. Green arrowheads indicate ZO-1 localization in control regions of the embryo, and red arrowheads indicate ZO-1 localization in regions expressing the injection marker. Scale bars, 20 μm. (D) Quantification of normalized ZO-1 intensity along the apical-to-basal axis of bicellular junctions. Error bars represent SEM. Control (*n* = 15, 6, 3), MO (*n* = 13, 5, 3).

the junctional localization of ZO-1 in mosaic regions where the Mgc MO was delivered (Figure 7, C and D, and Supplemental Figure S8F). These data suggest that Mgc is not required for proper TJ structure in the steady-state intact epithelium.

DISCUSSION

We used the intact vertebrate epithelium of *X. laevis* embryos to investigate Mgc's role in regulating localized Rho GTPase activity. We showed that Mgc's GAP activity spatially restricts accumulation of RhoA-GTP and Rac1-GTP in epithelial cells by down-regulating active RhoA at the cytokinetic furrow and both active RhoA and Rac1 at cell–cell junctions. We demonstrated that Mgc's GAP activity is required for successful cytokinesis, but phosphorylation at Ser-386 is not required. When Mgc's GAP activity was disrupted, we observed an increase in Rac1-GTP and RhoA-GTP at cell–cell junctions along with dynamic F-actin–rich accumulations that colocalize with RhoA-GTP. Finally, we showed that Mgc's GAP activity acts through RhoA to regulate proper AJ structure but is not required for TJ structure at steady state. Together these results indicate that Mgc's GAP activity is necessary to down-regulate the active populations of both RhoA and Rac1 at localized regions of epithelial cells, and this is required for successful cytokinesis and cell–cell junction structure and function (Figure 8).

Phosphorylation at Ser-386 does not switch the specificity of MgcRacGAP

It was reported that the isolated GAP domain of Mgc exhibits GAP activity primarily to Rac1 and Cdc42 and that phosphorylation of S386 by Aurora B kinase confers GAP activity toward RhoA (Minoshima *et al.*, 2003). Our data provide in vivo evidence supporting the conclusion that phosphorylation of MgcS386 does not switch Mgc's GAP specificity and is not required for successful cytokinesis. If phosphorylation at this site was important for Mgc's GAP activity toward RhoA, a nonphosphorylatable mutant (MgcS386A) would be predicted to cause abnormally increased RhoA-GTP accumulation. However, when endogenous Mgc was knocked down and replaced with MgcS386A, the cells exhibited normal RhoA-GTP accumulation and normal cytokinesis. In addition, our results raise the possibility that constitutive phosphorylation of S386 would disrupt cytokinesis and AJ structure, as a phosphomimetic mutant (MgcS386E) phenocopied the GAP-dead point mutant. MgcS386 is conserved in multiple species and is located two amino acids away

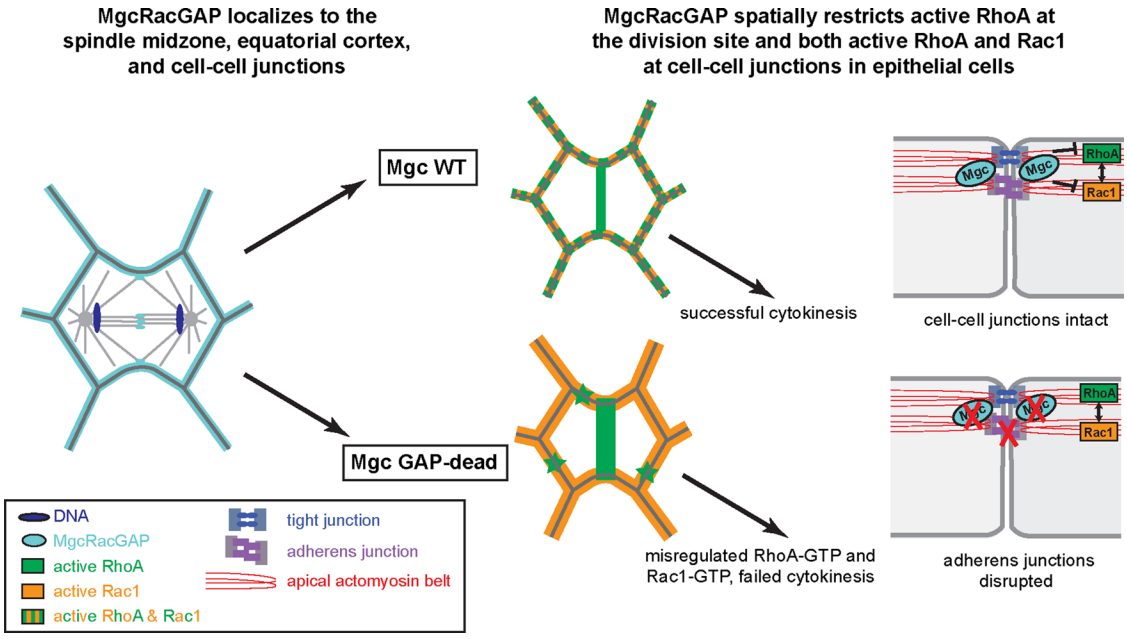

FIGURE 8: Model of how MgcRacGAP regulates active RhoA and Rac1 in dividing epithelial cells. Mgc's GAP activity is necessary to down-regulate the active population of RhoA at the division site and both RhoA and Rac1 at cell–cell junctions in epithelial cells, and failure to do so results in defects in cytokinesis and cell–cell junctions. Left, in dividing epithelial cells, Mgc is localized to the overlapping MTs of the spindle midzone, the equatorial cortex, and the apical surface of cell-cell junctions. Middle, in dividing control epithelial cells, active RhoA accumulates in a focused band at the cell equator, but in Mgc GAP-dead cells, equatorial RhoA activity is not focused. Both active RhoA and Rac1 accumulate at cell–cell junctions in control cells (indicated by stripes), but when Mgc's GAP activity is disrupted, Rac1-GTP is increased at bicellular and tricellular junctions, and RhoA-GTP coaccumulates with ectopic F-actin–rich junctional structures (indicated by stars). Right, Mgc's GAP activity is required for proper AJ structure. In Mgc GAP-dead cells, the intensity and apical polarity of AJs are disrupted. RhoA is known to regulate the apical actomyosin belt and AJ integrity. Expression of DN RhoA rescued the AJ defect in Mgc GAP-dead cells, suggesting that this defect was due to misregulated RhoA activity. In addition, RhoA and Rac1 can exhibit cross-talk to antagonize each other (indicated by double arrow).

from MgcR384, the conserved "arginine finger" residue that is essential for GAP activity (Supplemental Figure S1B). Both residues reside at the interface between the GAP and the GTPase (Rittinger *et al.*, 1997a,b). The placement of the serine residue with respect to the arginine finger is also conserved in some other Rho-family GAPs; however, phosphorylation at this site is not required for these GAPs to bind RhoA (Bastos *et al.*, 2012). In addition, Bastos *et al.* (2012) demonstrated that Mgc's in vitro GAP specificity was not modulated by phosphorylation at S386 for either recombinant Mgc protein or native Centralspindlin complexes immunoprecipitated from HeLa cells. Our studies support and extend these findings by providing in vivo data characterizing the effects of mutating S386 on the localized activity of RhoA and Rac1 in the intact epithelium.

In vivo GTPase targets of MgcRacGAP's GAP activity

Previous studies using diverse systems and approaches have led to conflicting conclusions regarding the specificity of Mgc's GAP activity toward RhoA and/or Rac1 (Minoshima *et al.*, 2003; Canman *et al.*, 2008; Miller and Bement, 2009; Bastos *et al.*, 2012; Loria *et al.*, 2012). RhoA is the primary Rho GTPase required for cytokinesis (O'Connell *et al.*, 1999; Jantsch-Plunger *et al.*, 2000; Davies and Canman, 2012). Our previous work in the large cells of blastula-stage *Xenopus* embryos showed that expression of MgcR384A results in abnormally broad RhoA activity zones and failed cytokinesis, supporting a role for Mgc in negatively regulating RhoA activity (Miller and Bement, 2009). Further, mathematical modeling suggested that the GAP activity required to focus the RhoA activity zone is localized at the cell equator rather then being global (Bement *et al.*, 2006). However, in vitro GAP assays indicate that Mgc exhibits efficient GAP activity toward Rac1 and Cdc42 but little GAP activity toward RhoA (Toure *et al.*, 1998; Jantsch-Plunger *et al.*, 2000; Minoshima *et al.*, 2003; Bastos *et al.*, 2012). Genetic studies in one-cell *C. elegans* embryos (Canman *et al.*, 2008) and *Drosophila* imaginal disks (D'Avino *et al.*, 2004) showed that Rac1 inhibition can partially suppress the effects of disrupting Mgc's GAP activity on cytokinesis. In addition, in adherent mammalian cultured cells, Rac1 signal is reduced at the cell equator in control cells (Yoshizaki *et al.*, 2003), but when GAP-dead Mgc is expressed, excess activated Rac1 accumulates at the cell equator, promoting increased cell–substrate adhesion, which antagonizes furrowing (Yoshizaki *et al.*, 2004; Bastos *et al.*, 2012).

Our data support the conclusion that in the physiologically relevant context of the intact vertebrate epithelium, Mgc can down-regulate both RhoA and Rac1: RhoA at the cleavage furrow and both RhoA and Rac1 at junctions. There may be a number of reasons for the conflicting findings in different experimental contexts. First, many of the key regulators of in vivo GAP activity are lacking in in vitro GAP assays, including the lipid bilayer, prenylation of Rho GTPases, and Rho guanine nucleotide dissociation inhibitors (Canagarajah *et al.*, 2004; Boulter *et al.*, 2010; Brill *et al.*, 2011; Tnimov *et al.*, 2012). For example, phospholipid binding to the C1 domain of β2-chimaerin activates its GAP activity (Canagarajah *et al.*, 2004), and interaction of

p190RhoGAP with phospholipids can switch its substrate specificity from RhoA to Rac1 (Levay *et al.*, 2013). Second, the colocalization of Mgc and RhoA-GTP at the cell equator may increase Mgc's efficiency as a RhoA GAP by facilitating access of Mgc to RhoA as a substrate. Third, the relative importance of different Rho GTPases and their regulators may differ in diverse cellular environments, including HeLa cells, one-cell *C. elegans* embryos, poorly adherent cells, or epithelial cells. For example, cells of the gastrula-stage *Xenopus* embryo are of similar size to HeLa cells, but cell–cell junctions with their neighbors prevail rather than the strong cell–substrate adhesions prominent in HeLa cells.

Although our data are consistent with a role for Mgc's GAP activity in down-regulating both Rac1 and RhoA in vivo, alternative explanations warrant future study. It is possible that Mgc may act indirectly on RhoA via cross-talk of Rho GTPases. Antagonism between Rac1 and RhoA has been described (Burridge, 1999; Machacek *et al.*, 2009). If Mgc primarily suppresses Rac1, antagonism would result in Mgc indirectly increasing RhoA. However, our results would imply a mechanism of GTPase cross-talk that is distinct from this mechanism, as both RhoA-GTP and Rac1-GTP increase at junctions when Mgc's GAP activity is disrupted. Additional GAPs, such as p190RhoGAP (Su *et al.*, 2003; Manukyan *et al.*, 2015) and MP-GAP (Zanin *et al.*, 2013) that act locally and/or globally could also be involved in regulating the spatiotemporal dynamics of RhoA-GTP.

MgcRacGAP's role at cell–cell junctions

RhoA and Rac1 are important regulators of cell–cell junction assembly and integrity (Braga *et al.*, 1997, 1999; Jou *et al.*, 1998; Machacek *et al.*, 2009; Terry *et al.*, 2010). We demonstrate that, in agreement with previous findings in cultured cells (Ratheesh *et al.*, 2012; Guillemot *et al.*, 2014), Mgc is localized to cell–cell junctions in both dividing and interphase cells in the *Xenopus* epithelium. Specifically, we find that Mgc is localized at the interface between the TJ and AJ, partially overlapping with each type of junction. Of importance, we demonstrate that Mgc's GAP activity is required for proper AJ structure. Expression of DN RhoA rescues the MgcR384A AJ phenotype, suggesting that the effect is due to unrestricted accumulation of RhoA-GTP. Guillemot *et al.* (2014) recently showed that Mgc regulates the development of the TJ barrier during TJ assembly; however, consistent with their findings, our results show that Mgc does not regulate the maintenance of TJ structure at steady state.

In summary, studying Mgc's role in regulating localized Rho GTPase activation in *Xenopus* embryos has provided novel information about how this GAP spatially restricts the accumulation of both RhoA-GTP and Rac1-GTP in intact vertebrate epithelial cells. Our results highlight the possibility that Mgc's primary Rho GTPase target may differ, depending on the adhesive environment of the cell.

MATERIALS AND METHODS

DNA constructs, mRNA preparation, and MgcRacGAP morpholino

Xenopus Mgc constructs, including the R384A point mutant and the 3xGFP-tagged construct, were described previously (Miller and Bement, 2009). MgcS386A, MgcR384K, and MgcS386E mutants were generated by QuikChange (Stratagene/Agilent Technologies, Santa Clara, CA) site-directed mutagenesis. A *Xenopus* E-cadherin construct was kindly provided by Pierre McCrea (University of Texas MD Anderson Cancer Center, Houston, TX). E-cadherin–3xmChe was generated by PCR amplifying the E-cadherin sequence and ligating it into the *Cla*I and *Xba*I sites in pCS2+/C-3XmChe. All constructs were confirmed by sequencing. The pCS2+/GFP-rGBD (probe for active Rho), pCS2+/GFP-pGBD (probe for active Rac), and pCS2+/mRFP-wGBD (probe for active Cdc42) probes were described previously (Benink and Bement, 2005; Miller and Bement, 2009), as were pCS2+/mChe-UtrCH (probe for F-actin; Burkel *et al.*, 2007), pCS2+/mChe-H2B (probe for DNA; Reyes *et al.*, 2014), pCS2+/mChe-membrane and pCS2+/GFP-membrane (Reyes *et al.*, 2014), and pCS2+/2XmChe-EMTB (probe for microtubules; von Dassow *et al.*, 2009). pCS2+/DN Rho and pCS2+/DN Rac were kindly provided by Tim Gomez (University of Wisconsin–Madison, Madison, WI). mRNAs were transcribed in vitro using an mMessage mMachine SP6 kit (Ambion/Life Technologies, Grand Island, NY). The Mgc 5′ UTR MO (Gene Tools, Philomath, OR), which was designed to target both alloalleles of *Xenopus* Mgc, was described previously (Miller and Bement, 2009).

Antibodies

The anti-*Xenopus* Mgc antibody was described previously (Miller and Bement, 2009). Other antibodies used were anti-mCherry (Ab125096 [mouse] and Ab167453 [rabbit]; Abcam, Cambridge, MA), anti-GFP (632381 [mouse], Clontech/Takara, Mountain View, CA; and A-6455 [rabbit], Invitrogen/Life Technologies, Grand Island, NY), anti-α-tubulin (DM1A, T9026; Sigma-Aldrich, St. Louis, MO), anti–β-catenin (Ab2365; Abcam), anti-E-cadherin (5D3-c; Developmental Studies Hybridoma Bank, Iowa City, IA), anti–claudin-5 (Ab53765; Abcam; note that the anti–claudin-5 antibody may cross-react with other claudins, so we refer to it simply as "anti-claudin" in the text and figures), and anti-ZO-1 (61-7300 [Rabbit]; Invitrogen). The mouse anti–ZO-1 antibody was a generous gift from Masahiko Itoh (Dokkyo Medical University, Mibu, Japan). Secondary antibodies used for immunostaining were Alexa 488– or Alexa 568–conjugated anti-mouse or anti-rabbit (Invitrogen). Secondary antibodies used for Western blotting were horseradish peroxidase (HRP)–conjugated anti-rabbit or anti-mouse (Promega, Madison, WI).

Xenopus embryos and microinjection

All studies conducted using *Xenopus* embryos strictly adhere to the compliance standards of the U.S. Department of Health and Human Services Guide for the Care and Use of Laboratory Animals and were also approved by the University of Michigan Committee on Use and Care of Animals. *Xenopus* embryos were collected, in vitro fertilized, and dejellied using methods described previously (Miller and Bement, 2009; Woolner *et al.*, 2009). Embryos were stored at different temperatures before injections to prolong the two-cell or four-cell stages (room temperature or 15 or 17°C) and then stored at 15°C in 0.1× Mark's modified Ringer solution, 1× = 100 mM NaCl, 2 mM KCl, 2 mM $CaCl_2$, 1 mM $MgCl_2$, and 5 mM 4-(2-hydroxyethyl)-1-piperazineethanesulfonic acid, pH 7.4. Embryos were microinjected as described previously (Reyes *et al.*, 2014). For knockdown and replacement experiments, all four cells at the four-cell stage were first injected with 5 nl of mRNA for indicated fluorescent probes (see later description); then all four cells were injected again with 5 nl of a mixture of MO (4.5 mM needle concentration), Mgc rescue construct (0.6 μg/ml needle concentration), and a fluorescent lineage tracer (see later description) and placed at 15°C for ~24 h until they reached gastrulation (Nieuwkoop and Faber stages 10–11). For overexpression experiments, embryos were injected at either the two- or four-cell stage with 5 nl of MgcWT or mutants (1.66 μg/ml needle concentration) and allowed to develop to blastula stage (Nieuwkoop and Faber stages 6–8). Needle concentrations for other mRNAs were as follows: Mgc-3xGFPs (1 μg/ml), GFP-rGBD (25 μg/ml), GFP-pGBD (15.6 μg/ml for gastrula and 0.25 mg/ml for blastula imaging), mRFP-wGBD (15.6 μg/ml), mChe-membrane

(10 µg/ml), GFP-membrane (10 µg/ml), mChe-H2B (20 µg/ml), mChe-UtrCH (10 µg/ml for gastrula and 0.71 mg/ml for blastula imaging), DN RhoA (0.48 µg/ml), DN Rac1 (0.6 µg/ml), E-Cad-3xmChe (8 µg/ml).

Embryo lysates and immunoblotting

Gastrula-stage embryos (Nieuwkoop and Faber stages 10–11) were lysed as previously described (Reyes *et al.*, 2014), with the following modifications: PHEME lysis buffer volume was 2.5 µl/embryo and did not include detergent. Samples were separated on 10% SDS–PAGE gels and transferred to nitrocellulose membranes. Membranes were probed with anti-Mgc (1:5000) or anti–β-tubulin (1:20,000) overnight at 4°C in 1× Tris buffered saline/0.1% Tween-20, pH 5.0, with 5% nonfat dry milk. HRP-conjugated secondary antibodies were applied at 1:5000 (for Mgc) or 1:10,000 for (β-tubulin). Membranes were developed using an ECL detection kit (32209; Pierce/Life Technologies, Grand Island, NY).

Immunostaining

Staining for endogenous Mgc. Albino embryos were injected with mChe-membrane as a lineage tracer with or without the Mgc 5′ UTR MO (4.5 mM needle concentration). Embryos were fixed at gastrulation by the trichloroacetic acid protocol described in Le Page *et al*. (2011) and Reyes *et al*. (2014), with the following changes: embryos were permeabilized in 1× phosphate-buffered saline/2% Triton X-100 (PBST) for 20 min at room temperature and then blocked in PBST with 5% fetal bovine serum (10082-139; Invitrogen) for 2–3 h at room temperature. Primary antibodies used were anti-Mgc (1:600), anti–E-cad (1:200), anti–ZO-1 (mouse; 1:300), and anti-mChe (1:200). Embryos were stained with 10 µg/ml 4′,6-diamidino-2-phenylindole (DAPI) (D1306; Invitrogen) in PBST for 30 min at room temperature and mounted in Vectashield mounting medium (H-1000; Vector Laboratories, Burlingame, CA).

Staining for β-catenin for Mgc knockdown and replacement. Embryos were injected as described, except that the lineage tracer was GFP-membrane. Embryos were fixed overnight with a paraformaldehyde/glutaraldehyde-based fixative following the protocol in Reyes *et al*. (2014). Primary antibodies were anti–β-catenin (1:200) and anti-GFP (1:200). Embryos were mounted in Murray's Clear for imaging.

Staining for claudin and ZO-1. Embryos were injected as described using GFP-membrane or mChe-membrane as a lineage tracer. Embryos were fixed for 2 h in 2% trichloroacetic acid following the protocol in Reyes *et al*. (2014), except that the secondary antibody was applied for 4 h at room temperature. Primary antibodies were rabbit anti-ZO-1 (1:200), anti-claudin-5 (1:50), anti-GFP (1:200), or anti-mChe (1:200). Embryos were mounted in Vectashield for imaging.

Live and fixed confocal microscopy

Fluorescence confocal images were collected on an inverted Olympus FluoView 1000 microscope equipped with a 60× supercorrected PLAPON 60XOSC objective (numerical aperture 1.4, working distance 0.12 mm) and FV10-ASW software. Live and fixed imaging was carried out as described previously (Reyes *et al.*, 2014).

Live-cell wounding

Embryos were injected into four cells at the four-cell stage with a probe for active Cdc42 (mRFP-wGBD) and incubated at 15°C for 20 h (Nieuwkoop and Faber stages 9.5–10). Images were collected using an Olympus FluoView 1000 microscope equipped with an auxiliary SIM scanner. Laser wounds were generated using the 405-nm SIM laser line at 37% power for 300 ms through a 60× objective. Single-plane movies were obtained before, during, and after the wound in order to capture the wound-healing response.

Quantification and analysis

Western blot intensity analysis. FIJI was used to quantify band intensity of each band from two independent anti-Mgc Western blots. The quantification was normalized to control Mgc levels.

Quantification of Mgc intensity in fixed cells. To measure Mgc intensity at the contractile ring, three circular regions of interest (ROIs; 2.5 µm in diameter) were placed along the cleavage furrow (in the center of the furrow and to the right and left of center) at ~50% ingression using Volocity (Perkin Elmer, Waltham, MA). For normalization, a background ROI of the same size was placed outside the cleavage furrow in the same cell and subtracted from the averaged cleavage furrow intensity value. The intensity value for control embryos was set to 1, and the intensity value for Mgc MO embryos was normalized to control. To measure Mgc intensity at cell–cell junctions, a line of 4 µm × 18 µm was drawn perpendicular to a cell–cell junction using ImageJ. The line was centered on the junction. Two lines were drawn per cell, and the average intensity for each point along the line was determined. The intensity values for each cell were normalized to background intensity by averaging the first five and last five data points of the line and subtracting this value from the averaged line scans. The intensity value for control embryos was set to 1, and the intensity value for Mgc MO embryos was normalized to control.

Cell width and percentage multinucleation measurements. Using Volocity, the width of each cell was measured vertically and horizontally across the cell and averaged. The percentage multinucleation was determined by first counting the cells per 230 µm × 230 µm image. The DAPI channel was then used to count how many cells displayed a single nucleus, two nuclei, or three or more nuclei by scanning through the volume of the cell; only cells for which nuclei could be clearly observed were included in the analysis.

Quantification of cytokinesis failure in live cells. Cytokinesis failure events were determined by observing cytokinesis in live-cell movies from embryos injected with either a probe for RhoA-GTP or Rac1-GTP along with mChe-UtrCH. A cell was determined to have failed cytokinesis if the contractile ring regressed at any point during cytokinesis.

Quantification of cytokinesis duration. The duration of cleavage furrow ingression was only recorded for cells that completed cytokinesis successfully. The start of cytokinesis was defined as when the F-actin contractile ring was first visible at the equatorial cortex. The end of cytokinesis was determined by the time at which the cleavage furrow had fully ingressed and cortical F-actin signal was separated between the two daughter cells.

Quantification of RhoA-GTP or Rac1-GTP intensity at the cleavage furrow. Three separate circular ROI's (2.5 µm in diameter) were placed along the cleavage furrow (middle of the zone and right and left sides of the zone) at ~25% ingression (early cytokinesis) using Volocity. For Rac1-GTP data analysis, the site of the cleavage

furrow was determined via the F-actin channel; then intensity measurements were made of Rac1-GTP signal at the identified locations. The data were normalized by placing a background ROI of the same size at a region adjacent to the cleavage furrow for each cell. The background ROI was subtracted from the averaged cleavage furrow intensity for each cell included in the analysis.

Measurements of RhoA-GTP and F-actin zone widths. The width of each cell was measured, and then three separate measurements were taken across the width of the RhoA-GTP or F-actin zone (middle of the zone and right and left sides of the zone) and averaged. All measurements were made in Volocity. The widths were normalized by calculating the ratio of the RhoA-GTP or F-actin zone to cell width. Early cytokinesis measurements were taken at ~25% cleavage furrow ingression, and late measurements were taken at ~75% cleavage furrow ingression.

Rac1-GTP intensity at cell vertices. The intensity of Rac1-GTP was measured in Volocity by positioning a circular ROI of 13-µm diameter at cell vertices of dividing cells at 75% ingression. A background ROI was positioned away from the cleavage furrow and cell–cell junctions. The data were normalized to background fluorescence by subtracting the background measurement from the cell vertices measurement for each cell.

Rac1-GTP line scans and full-width at half-maximum. A line of 4 µm × 18 µm was drawn perpendicular to the cell–cell junctions of dividing cells during late cytokinesis using ImageJ. The line was centered on the junction. Two lines were drawn per cell, and the average intensity for each point along the line was determined. For dividing cells, the line was placed across cell–cell junctions at polar regions of the cell to avoid the division site. The intensity values for each cell were normalized to background intensity by averaging the first five and last five data points of the line and subtracting this value from the averaged line scans. The Rac1-GTP junctional intensity reflects the peak value of the line scan. The full-width at half-maximum was determined by identifying the two points on the *x*-axis (width values) that are associated with the line scan at half of the maximum amplitude. The difference of the *x* values was calculated, and values of the full-width at half-maximum were plotted in a scatter plot.

Quantification of F-actin, RhoA, and Rac1 junctional accumulations. For kymographs, a rectangular ROI (25 µm × 10 µm) was cropped at the site of F-actin accumulations at cell–cell junctions. The cropped image was used to make montages of 20 frames (16-s time interval between frames) in ImageJ. Raw counts of F-actin accumulations were achieved by counting the F-actin–rich junctional accumulations that occur in a 500-s time interval in the top right quadrant of a 230 µm × 230 µm live movie. The total number of cells in the quadrant was counted for each embryo and used to determine the average percentage of F-actin–rich junctional accumulations that occur per cell per minute. Ten embryos were analyzed for each treatment group. The GTPase intensity at the site of an F-actin junctional accumulation was measured by identifying the location and timing of a junctional accumulation using the F-actin (red) channel, and then active GTPase intensity was measured at the corresponding site and time in the green channel and plotted over time.

Intensity line scans of junctional proteins. Side views of fixed embryos were analyzed in ImageJ using the freehand line function with line width of 10 pixels. A line was drawn along the apical-to-basal axis of a cell–cell junction, and the corresponding intensity values were recorded. A background intensity line was drawn adjacent to each cell–cell junction. Normalization was achieved by subtracting the background intensity from the junction intensity for each cell–cell junction included in the analysis.

Box-and-whisker plots. When data are presented as box-and-whisker plots, the whiskers represent the minimum and maximum, the top of the box represents the 75th percentile, the bottom of the box represents the 25th percentile, and the horizontal bar represents the median.

Statistical analysis. Unpaired Student's *t* tests were used to determine the statistical significance of each group pairwise compared with either control or MO + MgcWT as indicated. Statistics were calculated in GraphPad Prism software.

ACKNOWLEDGMENTS

We thank M. Itoh for the mouse anti–ZO-1 antibody; P. McCrea and T. Gomez for reagents; T. A. Arnold for help with cloning; R. E. Stephenson for providing mRNAs; M. L. Fekete for excellent technical support; and W. M. Bement, A. G. Goryachev, J. N. Bembenek, and members of our lab for helpful discussions and critical reading of the manuscript. This work was supported by a National Institutes of Health Grant (R00 GM089765) to A.L.M. E.B.B. was supported by a National Science Foundation Predoctoral Fellowship and a National Institutes of Health Cellular and Molecular Biology Training Grant (T32-GM007315). A.C.S. was supported by a Molecular Cellular and Developmental Biology Department Summer Research Fellowship. T.H. was supported by an International Postdoctoral Fellowship from the Japanese Society for the Promotion of Science.

REFERENCES

Bastos RN, Penate X, Bates M, Hammond D, Barr FA (2012). CYK4 inhibits Rac1-dependent PAK1 and ARHGEF7 effector pathways during cytokinesis. J Cell Biol 198, 865–880.

Benink HA, Bement WM (2005). Concentric zones of active RhoA and Cdc42 around single cell wounds. J Cell Biol 168, 429–439.

Bement WM, Benink HA, von Dassow G (2005). A microtubule-dependent zone of active RhoA during cleavage plane specification. J Cell Biol 170, 91–101.

Bement WM, Miller AL, von Dassow G (2006). Rho GTPase activity zones and transient contractile arrays. Bioessays 28, 983–993.

Boulter E, Garcia-Mata R, Guilluy C, Dubash A, Rossi G, Brennwald PJ, Burridge K (2010). Regulation of Rho GTPase crosstalk, degradation and activity by RhoGDI1. Nat Cell Biol 12, 477–483.

Braga VM, Del Maschio A, Machesky L, Dejana E (1999). Regulation of cadherin function by Rho and Rac: modulation by junction maturation and cellular context. Mol Biol Cell 10, 9–22.

Braga VM, Machesky LM, Hall A, Hotchin NA (1997). The small GTPases Rho and Rac are required for the establishment of cadherin-dependent cell-cell contacts. J Cell Biol 137, 1421–1431.

Brill JA, Wong R, Wilde A (2011). Phosphoinositide function in cytokinesis. Curr Biol 21, R930–934.

Burkel BM, von Dassow G, Bement WM (2007). Versatile fluorescent probes for actin filaments based on the actin-binding domain of utrophin. Cell Motil Cytoskeleton 64, 822–832.

Burridge K (1999). Crosstalk between Rac and Rho. Science 283, 2028–2029.

Canagarajah B, Leskow FC, Ho JY, Mischak H, Saidi LF, Kazanietz MG, Hurley JH (2004). Structural mechanism for lipid activation of the Rac-specific GAP, beta2-chimaerin. Cell 119, 407–418.

Canman JC, Lewellyn L, Laband K, Smerdon SJ, Desai A, Bowerman B, Oegema K (2008). Inhibition of Rac by the GAP activity of centralspindlin is essential for cytokinesis. Science 322, 1543–1546.

Danilchik MV, Brown EE (2008). Membrane dynamics of cleavage furrow closure in Xenopus laevis. Dev Dyn 237, 565–579.

Davies T, Canman JC (2012). Stuck in the middle: Rac, adhesion, and cytokinesis. J Cell Biol 198, 769–771.

D'Avino PP, Savoian MS, Glover DM (2004). Mutations in sticky lead to defective organization of the contractile ring during cytokinesis and are enhanced by Rho and suppressed by Rac. J Cell Biol 166, 61–71.
Fujiwara T, Bandi M, Nitta M, Ivanova EV, Bronson RT, Pellman D (2005). Cytokinesis failure generating tetraploids promotes tumorigenesis in p53-null cells. Nature 437, 1043–1047.
Godinho SA, Picone R, Burute M, Dagher R, Su Y, Leung CT, Polyak K, Brugge JS, Thery M, Pellman D (2014). Oncogene-like induction of cellular invasion from centrosome amplification. Nature 510, 167–171.
Goldstein AY, Jan YN, Luo L (2005). Function and regulation of Tumbleweed (RacGAP50C) in neuroblast proliferation and neuronal morphogenesis. Proc Natl Acad Sci USA 102, 3834–3839.
Green RA, Paluch E, Oegema K (2012). Cytokinesis in animal cells. Annu Rev Cell Dev Biol 28, 29–58.
Guillemot L, Guerrera D, Spadaro D, Tapia R, Jond L, Citi S (2014). MgcRacGAP interacts with cingulin and paracingulin to regulate rac1 activation and development of the tight junction barrier during epithelial junction assembly. Mol Biol Cell 25, 1995–2005.
Herszterg S, Leibfried A, Bosveld F, Martin C, Bellaiche Y (2013). Interplay between the dividing cell and its neighbors regulates adherens junction formation during cytokinesis in epithelial tissue. Dev Cell 24, 256–270.
Hirose K, Kawashima T, Iwamoto I, Nosaka T, Kitamura T (2001). MgcRacGAP is involved in cytokinesis through associating with mitotic spindle and midbody. J Biol Chem 276, 5821–5828.
Jantsch-Plunger V, Gonczy P, Romano A, Schnabel H, Hamill D, Schnabel R, Hyman AA, Glotzer M (2000). CYK-4: A Rho family gtpase activating protein (GAP) required for central spindle formation and cytokinesis. J Cell Biol 149, 1391–1404.
Jou TS, Schneeberger EE, Nelson WJ (1998). Structural and functional regulation of tight junctions by RhoA and Rac1 small GTPases. J Cell Biol 142, 101–115.
Lacroix B, Maddox AS (2012). Cytokinesis, ploidy and aneuploidy. J Pathol 226, 338–351.
Lavelin I, Geiger B (2005). Characterization of a novel GTPase-activating protein associated with focal adhesions and the actin cytoskeleton. J Biol Chem 280, 7178–7185.
Le Page Y, Chartrain I, Badouel C, Tassan JP (2011). A functional analysis of MELK in cell division reveals a transition in the mode of cytokinesis during Xenopus development. J Cell Sci 124, 958–968.
Levay M, Bartos B, Ligeti E (2013). p190RhoGAP has cellular RacGAP activity regulated by a polybasic region. Cell Signal 25, 1388–1394.
Li Z, Aizenman CD, Cline HT (2002). Regulation of rho GTPases by crosstalk and neuronal activity in vivo. Neuron 33, 741–750.
Loria A, Longhini KM, Glotzer M (2012). The RhoGAP domain of CYK-4 has an essential role in RhoA activation. Curr Biol 22, 213–219.
Machacek M, Hodgson L, Welch C, Elliott H, Pertz O, Nalbant P, Abell A, Johnson GL, Hahn KM, Danuser G (2009). Coordination of Rho GTPase activities during cell protrusion. Nature 461, 99–103.
Manukyan A, Ludwig K, Sanchez-Manchinelly S, Parsons SJ, Stukenberg PT (2015). A complex of p190RhoGAP and anillin modulates RhoGTP and the cytokinetic furrow in human cells. J Cell Sci 128, 50–60.
Matsuura A, Lee HH (2013). Crystal structure of GTPase-activating domain from human MgcRacGAP. Biochem Biophys Res Commun 435, 367–372.
Miller AL, Bement WM (2009). Regulation of cytokinesis by Rho GTPase flux. Nat Cell Biol 11, 71–77.
Minoshima Y, Kawashima T, Hirose K, Tonozuka Y, Kawajiri A, Bao YC, Deng X, Tatsuka M, Narumiya S, May WS Jr, *et al*. (2003). Phosphorylation by aurora B converts MgcRacGAP to a RhoGAP during cytokinesis. Dev Cell 4, 549–560.
Mishima M, Kaitna S, Glotzer M (2002). Central spindle assembly and cytokinesis require a kinesin-like protein/RhoGAP complex with microtubule bundling activity. Dev Cell 2, 41–54.
Miura K, Jacques KM, Stauffer S, Kubosaki A, Zhu K, Hirsch DS, Resau J, Zheng Y, Randazzo PA (2002). ARAP1: a point of convergence for Arf and Rho signaling. Mol Cell 9, 109–119.
Nishimura Y, Yonemura S (2006). Centralspindlin regulates ECT2 and RhoA accumulation at the equatorial cortex during cytokinesis. J Cell Sci 119, 104–114.
O'Connell CB, Wheatley SP, Ahmed S, Wang YL (1999). The small GTP-binding protein rho regulates cortical activities in cultured cells during division. J Cell Biol 144, 305–313.
Priya R, Yap AS, Gomez GA (2013). E-cadherin supports steady-state Rho signaling at the epithelial zonula adherens. Differentiation 86, 133–140.
Ratheesh A, Gomez GA, Priya R, Verma S, Kovacs EM, Jiang K, Brown NH, Akhmanova A, Stehbens SJ, Yap AS (2012). Centralspindlin and alpha-catenin regulate Rho signalling at the epithelial zonula adherens. Nat Cell Biol 14, 818–828.
Reyes CC, Jin M, Breznau EB, Espino R, Delgado-Gonzalo R, Goryachev AB, Miller AL (2014). Anillin regulates cell-cell junction integrity by organizing junctional accumulation of Rho-GTP and actomyosin. Curr Biol 24, 1263–1270.
Rittinger K, Walker PA, Eccleston JF, Nurmahomed K, Owen D, Laue E, Gamblin SJ, Smerdon SJ (1997a). Crystal structure of a small G protein in complex with the GTPase-activating protein rhoGAP. Nature 388, 693–697.
Rittinger K, Walker PA, Eccleston JF, Smerdon SJ, Gamblin SJ (1997b). Structure at 1.65 A of RhoA and its GTPase-activating protein in complex with a transition-state analogue. Nature 389, 758–762.
Shang X, Moon SY, Zheng Y (2007). p200 RhoGAP promotes cell proliferation by mediating cross-talk between Ras and Rho signaling pathways. J Biol Chem 282, 8801–8811.
Somers WG, Saint R (2003). A RhoGEF and Rho family GTPase-activating protein complex links the contractile ring to cortical microtubules at the onset of cytokinesis. Dev Cell 4, 29–39.
Su KC, Takaki T, Petronczki M (2011). Targeting of the RhoGEF Ect2 to the equatorial membrane controls cleavage furrow formation during cytokinesis. Dev Cell 21, 1104–1115.
Su L, Agati JM, Parsons SJ (2003). p190RhoGAP is cell cycle regulated and affects cytokinesis. J Cell Biol 163, 571–582.
Terry S, Nie M, Matter K, Balda MS (2010). Rho signaling and tight junction functions. Physiology (Bethesda) 25, 16–26.
Tnimov Z, Guo Z, Gambin Y, Nguyen UT, Wu YW, Abankwa D, Stigter A, Collins BM, Waldmann H, Goody RS, Alexandrov K (2012). Quantitative analysis of prenylated RhoA interaction with its chaperone, RhoGDI. J Biol Chem 287, 26549–26562.
Toure A, Dorseuil O, Morin L, Timmons P, Jegou B, Reibel L, Gacon G (1998). MgcRacGAP, a new human GTPase-activating protein for Rac and Cdc42 similar to Drosophila rotundRacGAP gene product, is expressed in male germ cells. J Biol Chem 273, 6019–6023.
von Dassow G, Verbrugghe KJC, Miller AL, Sider JR, Bement WM (2009). Action at a distance during cytokinesis. J Cell Biol 187, 831–845.
Wolfe BA, Takaki T, Petronczki M, Glotzer M (2009). Polo-like kinase 1 directs assembly of the HsCyk-4 RhoGAP/Ect2 RhoGEF complex to initiate cleavage furrow formation. PLoS Biol 7, e1000110.
Woolner S, Miller AL, Bement WM (2009). Imaging the cytoskeleton in live Xenopus laevis embryos. Methods Mol Biol 586, 23–39.
Yamada T, Hikida M, Kurosaki T (2006). Regulation of cytokinesis by mgcRacGAP in B lymphocytes is independent of GAP activity. Exp Cell Res 312, 3517–3525.
Yamada S, Nelson WJ (2007). Localized zones of Rho and Rac activities drive initiation and expansion of epithelial cell-cell adhesion. J Cell Biol 178, 517–527.
Yoshizaki H, Ohba Y, Kurokawa K, Itoh RE, Nakamura T, Mochizuki N, Nagashima K, Matsuda M (2003). Activity of Rho-family GTPases during cell division as visualized with FRET-based probes. J Cell Biol 162, 223–232.
Yoshizaki H, Ohba Y, Parrini MC, Dulyaninova NG, Bresnick AR, Mochizuki N, Matsuda M (2004). Cell type-specific regulation of RhoA activity during cytokinesis. J Biol Chem 279, 44756–44762.
Yuce O, Piekny A, Glotzer M (2005). An ECT2-centralspindlin complex regulates the localization and function of RhoA. J Cell Biol 170, 571–582.
Zanin E, Desai A, Poser I, Toyoda Y, Andree C, Moebius C, Bickle M, Conradt B, Piekny A, Oegema K (2013). A conserved RhoGAP limits M phase contractility and coordinates with microtubule asters to confine RhoA during cytokinesis. Dev Cell 26, 496–510.